Characterisation of anisotropic and non-linear behaviour of human skin

Meijer, R.

Award date:
2004

Characterisation of Anisotropic and Non-linear Behaviour of Human Skin

Riske Meijer

Final Report
WFW report 97.055

Professor:
J.D. Janssen

Coaches:
L.F.A. Douven (Philips Research Laboratories),
C.W.J. Oomens (Eindhoven University of Technology).

Research carried out from October 1996 to June 1997
at the Personal Care Institute of Philips Research Laboratories in Eindhoven.

Summary

At the Personal Care Institute of Philips Research Laboratories in Eindhoven, the shaving process is studied in order to improve existing shavers and develop new shaving systems. An important feature is the interaction between skin and apparatus. This is investigated by means of (*in vivo*) experiments as well as numerical simulations. Essential for these numerical simulations is the availability of a good constitutive model of human skin.

The aim of this research is to characterise the in-plane mechanical behaviour of human skin *in vivo*, employing the structural skin model of Lanir [Lanir, 1983]. The main features of the in-plane mechanical behaviour of human skin, anisotropy and non-linearity, are mainly determined by its collagen fibres. For this reason, only parameters of Lanir's Skin Model concerning the mechanical behaviour of the collagen fibres are estimated.

The *in vivo* orientation distribution and mechanical properties of collagen fibres in human skin were characterised using a mechanical method. This method is based on the confrontation of measured data from an experiment, with calculated data from the finite element model, eventually leading to the determination of some parameters of Lanir's Skin Model. For this purpose, two *in vivo* experiments were carried out on one piece of human skin at the inner side of the fore-arm, where the direction of stretch was applied in mutually perpendicular directions. During the experiments, reaction forces of the skin and the marker positions of different states of deformation were measured. The measured reaction forces of the skin were used for the determination of a set of parameters describing the mechanical properties of the collagen fibres. The marker positions were used for the determination of a set of parameters describing the collagen fibre orientation distribution in the reference state. The parameters converged to the same solutions from different initial guesses. The residuals of the reaction forces are in the expected order of magnitude. Therefore, the parameters describing the mechanical properties of the collagen fibres become reliable. However, the residuals of the marker positions are an order of magnitude larger than expected and exhibit structure, rather than randomness. The structure for both experiments differs. These are both indications that the constitutive model used for the characterisation of the in-plane mechanical behaviour of human skin *in vivo* exhibits modelling errors.

Additional information about the collagen fibre orientation during deformation was gained using the optical technique: Small Angle Light Scattering (SALS). In SALS, laser light is passed through a thin specimen, with a portion of incident light scattered due to the different refraction indices of the fibres and the surrounding matrix. In this research, SALS was applied at *in vitro* rat skin during uniaxial stretch. Verification experiments were carried out on a slice of mainly uniaxially orientated LCP material with a thickness of 40 μm. The SALS patterns, measured with a CCD camera, were used for the quantification of the fibre orientation distributions. From the results of the verification experiments, it appears that it is possible to determine the preferred fibre orientation. The results of the *in vitro* experiments show that the CCD camera used is not sensitive enough to determine the preferred collagen fibre orientation of the skin samples with a thickness of 380 μm.

Contents

Notation

a	scalar
$\underset{\sim}{a}$	column of scalars
$\vec{a}$	vector
$\underset{\sim}{\vec{a}}$	column of vectors
$E(a)$	expected value of a
$\hat{a}$	estimate of a
$\overline{a}$	mean of a
$\underline{A}$	matrix
$\underline{A}^T$	transpose of matrix
$\underline{A}^{-1}$	inverse of matrix
$\underline{I}$	unit matrix
$\boldsymbol{A}$	second order tensor
$\boldsymbol{A}^c$	conjugate of tensor
$\boldsymbol{A}^{-1}$	inverse of tensor
$\boldsymbol{I}$	unit tensor

Chapter 1

Introduction

1.1 Problem Definition

At the Personal Care Institute of Philips Research Laboratories in Eindhoven, the shaving process is studied. The aim of this study is to improve existing shavers and develop new shaving systems in order to enhance the shaving performance. An important feature is the interaction between skin and apparatus. This is investigated by means of (*in vivo*) experiments as well as numerical simulations. Essential for these numerical simulations is the availability of a good constitutive model of human skin. The constitutive model currently used is a hyperelastic model. This model incorporates non-linear isotropic elastic behaviour and is routinely used to model the mechanical behaviour of rubber materials. However, when simulating more complex deformations of the skin, the results of this hyperelastic model are non-consistent. Lanir's Skin Model is a constitutive model which is able to describe the mechanical behaviour of skin more accurately [Lanir, 1983]. A numerical-experimental approach has been made to characterise the mechanical behaviour of human skin *in vivo*, employing Lanir's Skin Model [Voorden, 1996]. Voorden's work was limited to the characterisation of the *in vivo* configuration of collagen fibres in skin. However, Lanir's Skin Model contains more parameters to be determined by experiments. In this research we will try to estimate this extended set of parameters.

1.2 Structure and Mechanical Properties of Human Skin

Skin is a complex material. It has a stratified structure consisting of three main layers: an exterior cellular covering called the epidermis, beneath this, a dense connective tissue layer called the dermis and a fatty layer called hypodermis or subcutis. Figure 1.1 shows a schematic representation of the structure of skin. The thickness of each layer varies in different parts of the body, but the dermis is normally one order of magnitude thicker than the epidermis. In most areas, the epidermis varies from 0.07 *mm* to 0.12 *mm* and the dermis from 0.3 *mm* to 4 *mm* [Savenije, 1982]. The palms of the hands and the soles of the feet are the exceptions.

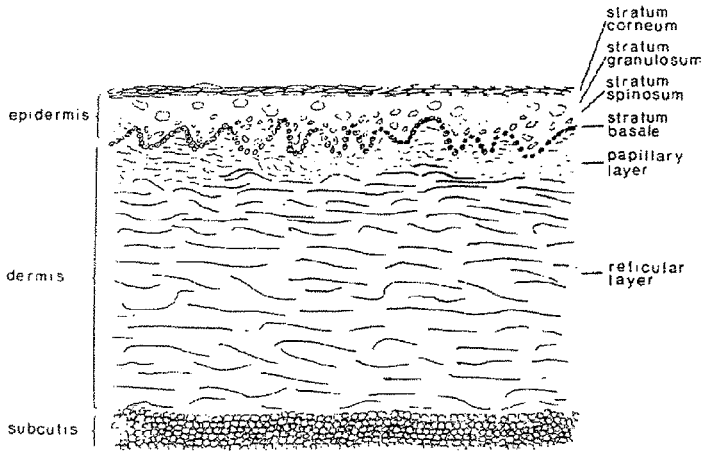

Figure 1.1: Schematic cross-section of skin.

The epidermis acts as a prime barrier against molecular transport of substances through the skin. The epidermis can be divided into an inner layer of viable cells and an outer layer of death horny cells, the stratum corneum. In most parts of the body, the thickness of this outer layer varies from 0.008 *mm* to 0.013 *mm* [Savenije, 1982].

The dermis is subdivided into two structurally distinctive layers: the papillary layer and the reticular layer. The papillary layer forms about 10% of the full dermis thickness [Manschot, 1985]. It follows the contours of the wavy and fingerlike folded epidermal-dermal juncture which ensures that the epidermis cannot slide over the dermis. The papillary layer consists of an open network of delicate fibres of collagen, elastin and minute quantities of reticulin. Below this the reticular layer, mainly composed of densely intertwined coarse collagen fibres, forms the main structural body of the skin. The mechanical behaviour of skin depends primarily on the response of the constituents of this layer. Its main constituents are collagen and elastin fibres embedded in a matrix of amorphous ground substance.

Collagen accounts for about 75% of the fat-free dry weight [Montagna, 1965], corresponding to 30% of the total skin volume [Manschot, 1985]. Their width ranges from 1 to 40 μm. Under the light microscope the collagen fibres resemble an irregular meshwork, oriented roughly parallel to the epidermis [Finlay, 1969], [Brown, 1972]. Characteristic of the collagen fibres is their undulation. During stretch these originally undulated fibres unfold and orientate into the direction of stretch. Examination of the collagen molecule has shown that at least five different types exist [Oxlund, 1983]. For the mechanical properties of skin only type I and III are of interest. Almost 90% of the dermal collagen fibres are of type I. Type III collagen is found in the papillary layer and in fibres surrounding the reticular layer [Smith et al., 1982]. Reticulin consists basically of type III collagen. Investigations have demonstrated the high strength, low extensibility and viscoelastic properties of collagen. The elastic modulus of collagen is approximately $1 \cdot 10^8\ N \cdot m^{-2}$ [Savenije, 1982].

Elastin fibres are less abundant in skin, they constitute about 2% of the total skin volume [Manschot, 1985]. They vary in width from 0.5 to 8 μm and form an extensive network around the thicker collagen fibres [Finlay, 1969], [Brown, 1972]. Elastin's characteristic mechanical property is its low-range elastic extensibility and little viscoelastic effects. They are believed to act as energy storage and, after unloading, they pull the collagen back to their original position [Manschot, 1985]. The elastic modulus of elastin is approximately $1 \cdot 10^6\ N \cdot m^{-2}$ [Savenije, 1982].

The ground substance is a complex matrix and can be characterised as a semi-fluid amorphous material. Its main constituents are glycoaminoglycans (GAG) that are able to bind water in a molecular form. The ground substance is also thought to be partly responsible for the viscous part of the mechanical response of skin [Brown, 1971].

The reticular layer is loosely connected to the hypodermis. Since the hypodermis is supposed to have a fixed lower surface, the influence of this layer on stretching of skin could only result from shearing.

Although the thickness of the hypodermis amounts to 5 times the dermis thickness, its contribution to the in-plane mechanical behaviour of skin can be neglected [Manschot, 1985]. Non-fibrous components like hair follicles, glands and blood vessels are enmeshed in fine fibrillar systems which separate them from the coarse dermal fibre network [Brown, 1971].

The load deformation relationship for whole skin tested in uniaxial tension can be described by four stages of extension, as shown in figure 1.2a. In the initial stage of extension the collagen fibres unfold causing elastic mechanical behaviour with low stiffness. In the second stage more and more fibres become aligned in the direction of the load, resulting in non-linear behaviour. The slope of the almost linear third stage of extension is similar to that of pure collagen. The final stage of the load deformation curve corresponds to yielding and rupture of the skin [Daly, 1966]. The amount of extension at which Stage II is reached depends on body site, derection of stretch and age. Figure 1.2b shows a schematic representation of the collagen fibre arrangements in the four stages of extension.

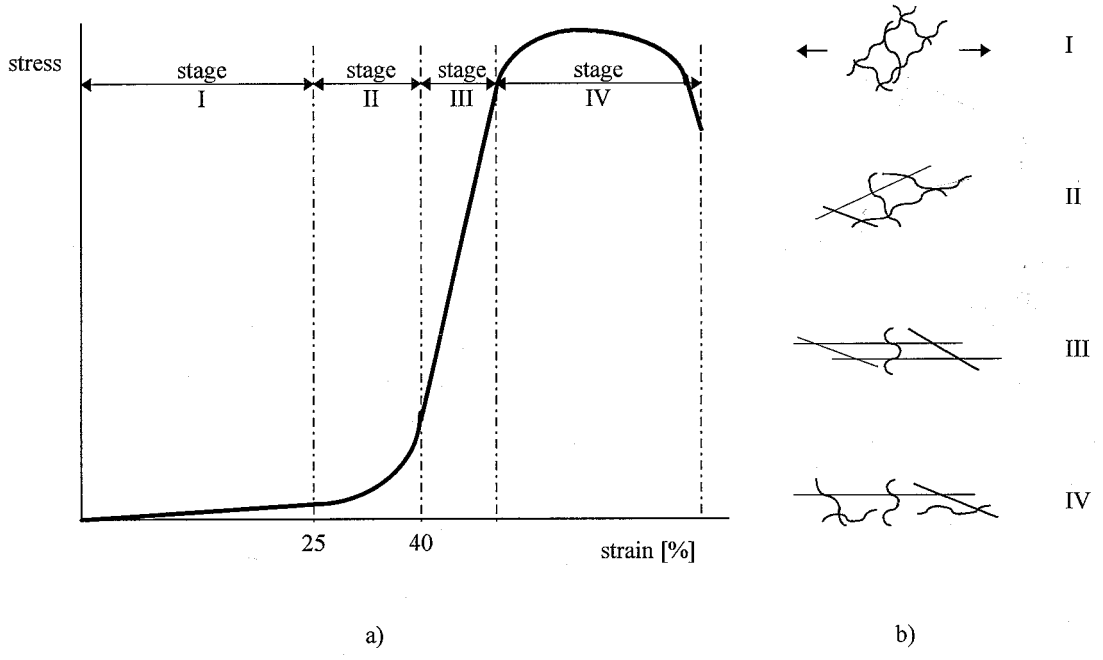

Figure 1.2: a) Stress-strain graph obtained in a destructive tensile test of human skin *in vitro* illustrating the different stages of extension [Daly, 1966]. The values for the strain are not exact, they only give an indication.
b) Schematic representation of the collagen fibre arrangement in the stages of extension. The arrows point in the loading direction.

The natural tension present in skin *in vivo* is called pre-tension. The amount and orientation of the pre-tension is distributed inhomogeneous over the body. In most areas, skin is in a state of anisotropic tension. In a study of skin tension, Langer discovered that puncturing the skin with a sharp conical instrument produces an oval shaped wound. A series of punctures, each made in the direction of the long axis of the preceeding puncture, results in a distinct pattern of lines, the so-called Langer's Lines. In figure 1.3, the distribution of Langer's Lines at the inner side of a man's arm is schematically drawn. Examination of skin sections made in two planes, one at right angles and one exactly parallel to the long axis of a linear puncture wound, shows a striking difference in structure. Sections at right angles to the long axis show a marked preponderance of collagen and elastin fibres cut transversely. Sections parallel to the long axis show a similar preponderance of fibres running longitudinally. The direction of Langer's Lines demonstrates the direction of the majority of the fibres, so that the whole pattern becomes a visible demonstration of the lay-out of these fibres [Langer, 1861], [Cox, 1941].

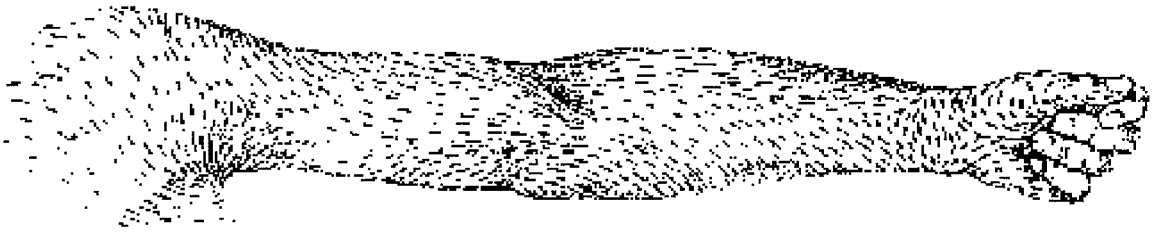

Figure 1.3: Distribution of Langer's Lines at the inner side of a man's arm [Langer, 1861].

Summarising, it can be stated that the overall response of skin to macroscopic deformation leads to **inhomogeneous, viscoelastic, non-linear** and **anisotropic** mechanical behaviour. Furthermore, the mechanical behaviour of human skin depends on age, sex, and humidity. The age-related dependence of biomechanical behaviour is a function of an increased crosslinking of collagen fibres, the degradation of the elastin network and changes in the ground substance [Manschot, 1985], resulting in a decreased extensibility of skin. The humidity of the environment influences the stiffness of the stratum corneum. Its stiffness can vary from $2 \cdot 10^9\ N \cdot m^{-2}$ for dry stratum corneum (relative humidity of 30%) to $3 \cdot 10^6\ N \cdot m^{-2}$ for wet stratum corneum [Manschot, 1985].

1.3 Characterisation of the Mechanical Behaviour of Skin

The aim of this study is to characterise the in-plane mechanical behaviour of human skin *in vivo*. For this purpose Lanir's Skin Model is employed [Lanir, 1983]. The main features of the stress-strain relationships in skin: anisotropy and non-linearity, are fully accounted for by Lanir's Skin Model. It is a model based on structural grounds, assuming that the tissue's response is the sum of the responses of its constituents. Hence, if the constituents' structure, their mechanics and interactions are known, the overall tissue's response can be evaluated.

Since the dermis is two orders of magnitude thicker than the stratum corneum and the dermis is loosely connected to the hypodermis, the dermis is assumed to dominate the in-plane mechanical behaviour of human skin. The main features of the in-plane mechanical behaviour of human skin, anisotropy and non-linearity, are mainly defined by its collagen fibres. For this reason, only the material parameters concerning the mechanical behaviour of the collagen fibres are estimated.

The *in vivo* configuration and mechanical properties of collagen fibres in human skin will be characterised using a mechanical method. This method is based on Hendriks' identification method [Hendriks, 1991]. The identification method has proven to be succesfull in numerous investigations concerning the investigation of complex materials [Oomens et al., 1993], [Ratingen, 1994]. It is based on the confrontation of measured data from an experiment with calculated data obtained by a finite element model, eventually leading to an estimation of the some material parameters of a constitutive model.

Because the mechanical method is rather complex, additional information about the collagen fibre orientation during deformation is gained by another experimental method. The collagen fibre orientation distribution in *in vitro* tissues can be characterised using an optical technique called Small Angle Light Scattering (SALS), [Kronick & Buechler, 1986], [Sacks & Chuong, 1992]. In SALS, laser light is passed through a thin specimen, with a portion of incident light scattered due to the different refraction indices of the fibres and the surrounding matrix. By analysing the distribution of scattered light, it is possible to quantify the in-plane orientation distibution of collagen fibres.

Eventually, the skin model employed and the methods used for the characterisation of the in-plane mechanical behaviour of human skin *in vivo* are discussed.

1.4 Overview

In the next chapter, Lanir's Skin Model and the theories of the mechanical and the optical methods are described. Chapter 3 describes the characterisation of human skin *in vivo* employing the mechanical method. Chapter 4 describes the characterisation of collagen fibre orientation during deformation of skin *in vitro* employing the optical method. Finally, in chapter 5, conclusions are drawn from the results obtained by the experiments and recommendations are made for future research.

Chapter 2

Theory

In this chapter, Lanir's Skin Model and the methods used for the characterisation of some of its material parameters are described.

2.1 Lanir's Skin Model

Lanir's Skin Model is a constitutive model for the skin employing a structural approach. A structural skin model enhances our understanding of the tissue's function deformation behaviour. In tissue characterisation, structural models have a distinct advantage since the structure is often known or can be investigated. However, structural models often contain a lot of parameters, making the model rather complex. In case of implementation in a finite element code, this can result in an increase of computing effort. In order to reduce the computing effort, we will restrict ourselves to the characterisation of the in-plane mechanical behaviour.

2.1.1 Assumptions

The mechanical behaviour of skin is assumed to be dominated by the dermis; the influence of the epidermis and hypodermis are neglected. In Lanir's Skin Model, structure is defined in terms of the fibres' orientation [Lanir, 1983]. In flat tissues, the orientation distribution of each fibre type, k, can be prescribed by a density distribution function $R_k(\theta)$, where the argument is the polar angle θ. Hence, $R_k(\theta)\cdot d\theta$ is the fraction of fibres oriented between (θ) and $(\theta + d\theta)$. The continuous orientation distribution function $R_k(\theta)$ gives a more accurate description of the fibre orientation distribution than a discrete orientation distribution function, as used by Voorden [Voorden, 1996]. The continuous orientation distribution functions used in this research are defined in section 2.1.3.

The following assumptions are made in employing Lanir's Skin Model:

- Each fibre is thin and perfectly flexible. It has no compressive strength and if contracted will buckle under zero load. The fibres that are undulated do not carry load until they are completely straightened.
- If a fibre is stretched, it is subjected to a uniaxial strain which is the tensorial transformation of the overall strain in the fibre's direction (affine deformation).
- The fibres are linear elastic.
- Upon stretching, the fraction of fibres that are straightened and stretched rises. This provides non-linear behaviour.
- Skin is incompressible.
- The unfolding and rotating of the fibres during deformation squeezes the matrix. The matrix's response is through hydrostatic pressure only.

2.1.2 Constitutive Model

The stress-strain relation is described with:

$$\sigma = \tau - pI, \tag{2.1}$$

where σ is the Cauchy stress tensor, τ the so-called extra stress tensor, p a hydrostatic pressure and $\boldsymbol{I}$ the second order unit tensor. The mechanical behaviour of fibres is accounted for in τ and the contribution of the groundsubstance is accounted for in p. The stress-strain relation defined by Feron [Feron, 1993] is revised for an in-plane continuous fibre distribution:

$$\sigma = J^{-1}\sum_k S_k \int_0^{\pi} (R_k(\theta)\frac{1}{\lambda(\vec{r}_0)} f_k^*\left(\lambda(\vec{r}_0)\right)\boldsymbol{F}\cdot\vec{r}_0\vec{r}_0\cdot\boldsymbol{F}^c)d\theta - pI \tag{2.2}$$

with:

- $\boldsymbol{F}$ the deformation tensor, and $J = \det(\boldsymbol{F})$ a measure for the volume strain,
- $R_k(\theta)\cdot d\theta$ the fraction of all fibres of type k oriented between (θ) and $(\theta + d\theta)$ in the reference state. The function $R_k(\theta)$ should satisfy the normalisation condition:

$$\int_0^{\pi} R_k(\theta)d\theta = 1. \tag{2.3}$$

- $\vec{r}_0$ a unit vector tangent to the fibre in reference configuration defined by:

$$\vec{r}_0(\theta) = cos(\theta)\vec{e}_x + sin(\theta)\vec{e}_y, \tag{2.4}$$

- $\lambda(\vec{r}_0)$ the elongation ratio of fibres oriented in the direction $\vec{r}_0$ in the reference state,
- S_k, the volume fraction of fibre type k out of the total volume,
- $f_k^*\left(\lambda(\vec{r}_0)\right)$ the load per unit undeformed cross-sectional area, which also accounts for the undulation of fibres according to a normal distribution $N(\mu_k, \sigma_k)$. This function is outlined in section 2.1.4.

This model is implemented [Feron, 1993] in the finite element code MARC [MARC, 1994]. A 4-node bilinear quadrilateral element is used. The use of the hydrostatic pressure as unknown results in a mixed finite element formulation, where the incompressibility constraint is forced using the penalty function method. A Newton-Raphson iteration scheme is applied to solve the system of non-linear equations.

2.1.3 Fibre Orientation Distribution Functions

The following orientation distribution function is chosen for the collagen fibres [Lanir, 1996]:

$$R_c(\theta) = A\cdot cos^4(\theta - C_2) + B, \tag{2.5}$$

where A and B are constants. By requiring that the function is symmetric, cyclic, smooth and should satisfy the normalisation condition for density distribution functions (see equation 2.3), equation (2.5) attains the form:

$$R_c(\theta) = 1/\pi + C_1(cos^4(\theta - C_2) - 0.375). \tag{2.6}$$

The restiction $R(\theta) \geq 0$ for all θ imposes limits on C_1, namely $0 \leq C_1 \leq 0.849$. The orientation assosiated with the angle C_2 ($0 \leq C_2 \leq \pi$) is the direction of physical symmety for the fibrous structure or the preferred fibre orientation.

The orientation distribution of elastin is assumed to be isotropic and can thus be defined by:

$$R_e(\theta) = 1/\pi\,. \tag{2.7}$$

2.1.4 Stress-Elongation Law for Undulated Fibres

Fibres are assumed to be perfectly thin and flexible, therefore they have no compressive stiffness. For straightened fibres, linear elastic behaviour is assumed. These assumptions lead to the stress-elongation relation for straightened fibres given by:

$$f_k(\lambda) = \begin{cases} 0 & \text{for } \lambda > 0 \\ K_k(\lambda - 1) & \text{for } \lambda > 1 \end{cases}, \tag{2.8}$$

with K_k the stiffness constant of fibre type k.

In order to incorporate the undulation behaviour of fibres, this stress-elongation relation is adjusted. Figure 2.1 shows three different states of deformation that may occur for a fibre, when the skin is stretched.

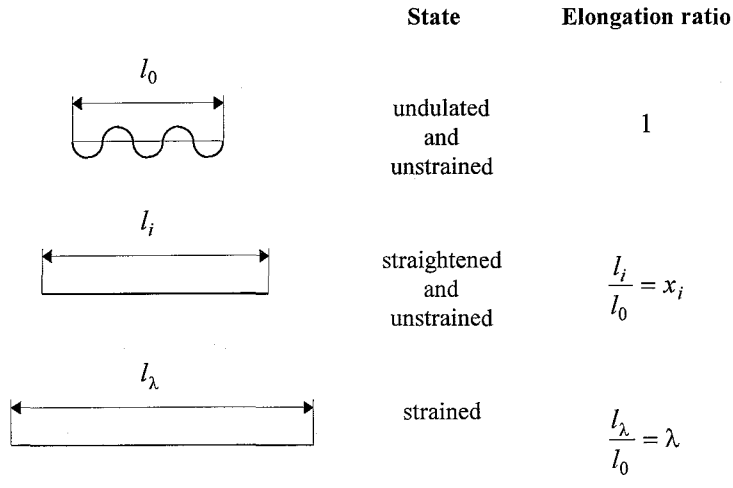

Figure 2.1: Fibre shapes at different states of deformation.

Fibre i remains unstraightened until it has an elongation ratio of $x_i = l_i / l_0$. Here, l_0 is the fibre length along $\vec{r}_0$ in the undulated, unstrained state and l_i the fibre length when it is straightened and unstrained. When the fibre is stretched further, the fibre will be strained and able to carry load. In figure 2.2, the stress-elongation relation for fibre i is shown.

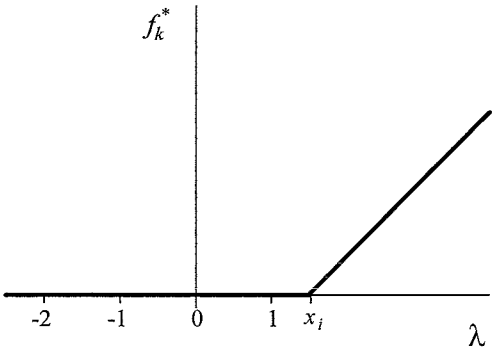

Figure 2.2: Stress-elongation relation for undulated fibre *i*.

To describe the behaviour of an undulated fibre a new variable, the effective elongation ratio λ_i^*, is introduced:

$$\lambda_i^* = \frac{l_\lambda}{l_i} = \frac{l_\lambda}{l_0}\frac{l_0}{l_i} = \frac{\lambda}{x_i}. \tag{2.9}$$

The distribution of the undulation amongst fibres of type *k* is expressed in the form of an undulation density distribution function $D_{k,\vec{r}_0}(x)$. The undulation of fibres is assumed to be normally distributed, therefore this function is given by:

$$D_{k,\vec{r}_0}(x) = \frac{1}{\sigma_{k,\vec{r}_0}\sqrt{2\pi}} e^{\frac{-(x-\mu_{k,\vec{r}_0})^2}{2\sigma_{k,\vec{r}_0}^2}}, \tag{2.10}$$

where $\mu_{k,\vec{r}_0}$ is the mean elongation ratio of fibres of type *k* in the reference state and $\sigma_{k,\vec{r}_0}$ the standard deviation.

Now, the load per unit undeformed cross-sectional area that is contributed by fibres of type *k* oriented in direction $\vec{r}_0$ and straighten between a stretch of *(x)* and *(x + dx)* can be described by $D_{k,\vec{r}_0}(x) f_k(\frac{\lambda}{x})dx$.

Suppose, $a_{k,\vec{r}_0}$ is the portion of fibres of type *k* oriented in direction $\vec{r}_0$ that is already straightened in reference configuration. Then, the total load per unit unstrained cross-sectional area contributed by all fibres of type *k* in direction $\vec{r}_0$, with different straightening strain, can be formulated by:

$$f_k^*\left(\lambda(\vec{r}_0)\right) = a_{k,\vec{r}_0} f_k(\lambda) + \int_{x=1}^{\lambda} D_{k,\vec{r}_0}(x) f_k(\frac{\lambda}{x})dx. \tag{2.11}$$

The collagen fibres are assumed to be undulated. So, the load per unit unstrained cross-sectional area by all collagen fibres in direction $\vec{r}_0$ is defined by equation (2.11). The elastin fibres are assumed to be already strained in reference configuration. In equation (2.11) this can be modelled by choosing the mean elongation ratio for elastin fibres, $\mu_{e,\vec{r}_0}$, 0 and its standard deviation small, for example 0.2, so that the portion of elastin fibres oriented in direction $\vec{r}_0$ that is already straightened in reference configuration, $a_{e,\vec{r}_0}$, is about 1. This means that all elastin fibres and the portion of collagen fibres defined by $a_{c,\vec{r}_0}$ account for the pre-tension in skin in the employed constitutive model (equation 2.2).

2.2 Mechanical Method

For the characterisation of the *in vivo* orientation distribution and the mechanical properties of the collagen fibres in human skin, a mechanical method is used which is based on Hendriks' identification method [Hendriks, 1991]. The purpose of Hendriks' identification method is to estimate some material parameters of a constitutive equation.

Hendriks' identification method is extremely suitable for characterising anisotropic and inhomogeneous materials like biological tissue for several reasons:

- As inhomogenous strain fields are allowed, more freedom in the design of the experimental set-up is gained, which is especially convenient for *in vivo* measurements.
- Moreover, inhomogeneous strain fields contain more information about the material behaviour than homogeneous strain fields.

The identification method is based on the use of three elements:

1) measurements of field data from an experiment,
2) finite element modelling of the experiment,
3) an iterative scheme to obtain estimates for the material parameters in the constitutive model employed.

These three elements and their mutual connections are schematically presented in figure 2.3.

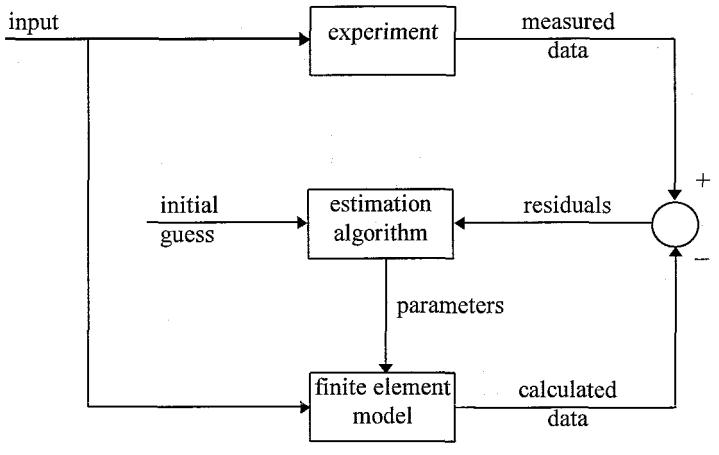

Figure 2.3: Diagram for the identification method [Hendriks, 1991].

In the following sections, the three elements are described for the mechanical method.

2.2.1 Data Measurements

A common method for obtaining strain field distributions is to place markers on the surface of the specimen and impose a certain state of deformation. The positions of the markers can be determined with image analysis software.

To obtain more information about the degree of undulation of the collagen fibres, information about the absolute stiffness is required. This can be obtained by measuring reaction forces required to deform the skin. If skin is stretched *in vivo*, an undefined, rather large area is deformed. In order to limit the deformation to a certain area, the skin under investigation needs to be isolated from its surrounding.

A disadvantage of *in vivo* experiments is that they can only be carried out on the surface of the specimen. This means that the data measurements are only relevant, if the surface of the specimen (epidermis) acts the same as its underlying layer (dermis).

2.2.2 Finite Element Modelling

For finite element modelling of the experiment, the finite element code MARC [MARC, 1994] is used. A finite element model of the experiment is made. The kinematic boundary conditions are based on the imposed deformation and the isolation of the specimen. The positions of the markers can be used as nodes in the finite element model. For the finite element calculations, a given set of parameters is needed.

2.2.3 Parameter Estimation

The essential part of the mechanical method is the iterative procedure that is used to adjust the parameters of the constitutive equation of Lanir's Skin Model (see equation 2.2). The simulation of the experiment results in a set of calculated data which can be compared with a set of data measured in the experiment. The difference (residuals) between the two sets can be used in order to adjust the parameters. The algorithm employed in this research is based on a constrained sequential maximum-likelihood approach [Starmans, 1994]. The minimisation procedure used takes in account possible equality and inequality constrains as well as possible linear dependencies of the parameters. The algorithm employed is described in appendix A.

2.3 Optical Method

In order to characterise the in-plane orientation distribution of collagen fibres in skin during deformation, Small Angle Light Scattering (SALS) is used. SALS is an optical technique allowing structural characterisation of many fibrous materials. Advantages of this method are that it is fast, accurate and inexpensive. A disadvantage of this method is that, in case of biological tissues, the sample has to be excised. Previous studies using SALS for characterising the mechanical behaviour of *in vitro* biological tissues are: the characterisation of the collagen fibre architecture in the canine diafragmatic tendon, a soft collageneous membrane [Sacks & Chuong, 1992], and for leather purposes, the examination of the fibre orientation in stretched calfskin [Kronick & Buechler, 1986]. An example of an application of SALS on other fibrous tissues is the determination of paper sheet fibre orientation distributions [Yang et al., 1987].

In this research, SALS is applied on, undeformed and deformed, isolated skin. In the next sections, the SALS method used for measuring the in-plane collagen fibre orientation distribution is described.

2.3.1 Light Scattering by Fibres

In SALS, a coherent beam of light, produced by a laser, is positioned perpendicular to the plane of a thin, translucent specimen. Passing through the specimen, a ray is attenuated in amplitude and retarded in phase. When a ray passes through an element with a higher refraction index, it will be diffracted more. Figure 2.5 shows a light ray diffracted by a fibre in the specimen.

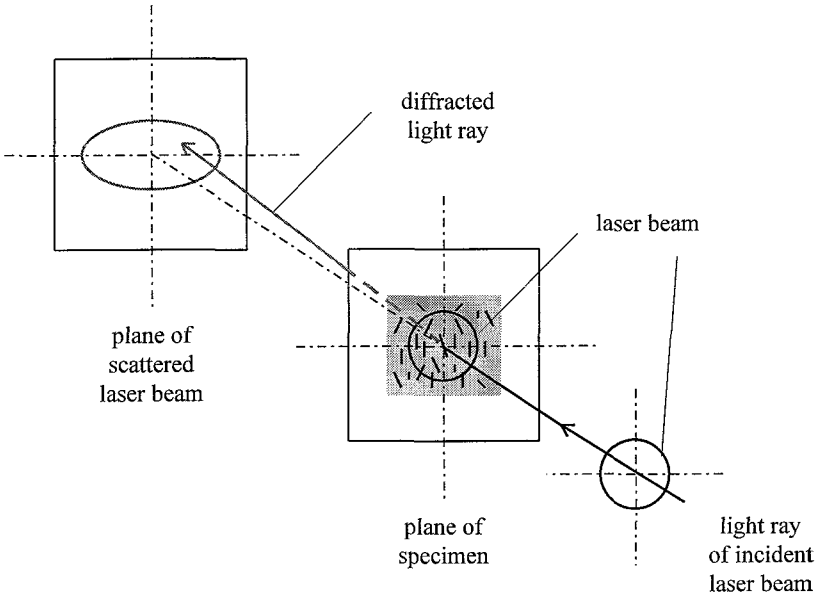

Figure 2.5: Diffraction of light by a fibre in a specimen.

The transmitted light scatters at a plane behind the specimen. Since light is diffracted in a direction perpendicular to the long axis of a fibre, the preferred direction of scattering will be perpendicular to the preferred orientation of the fibres. The light intensity in this scattered pattern is the square of the amplitude of the diffracted light [Hecht, 1987]. Because phase differences in the transmitted light are not relevant, the light intensity in the scattered pattern gives information about the in-plane collagen fibre orientation distribution.

2.3.2 Quantification of Fibre Orientation Distribution

Light intensity detectors (photodiodes) can be used to detect the SALS pattern. Using image analysis software, the detected pattern can be converted into an intensity plot, as shown in figure 2.6. The intensity is highest in the middle. This is due to the irradiance of the laser beam which is distributed Gaussian [Hecht, 1987]. From the intensity plot, the fibre orientation distribution can be quantified. Here, Lanir's fibre orientation distribution function for collagen fibres (see section 2.1.3) can be used to quantify the fibre orientation distribution in the specimen.

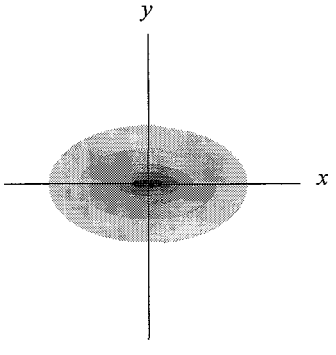

Figure 2.6: Intensity plot of the Small Angle Light Scattering pattern.

Chapter 3

Mechanical Behaviour of Human Skin In Vivo

In this chapter, the mechanical behaviour of human skin *in vivo* is characterised using the mechanical method as described in section 2.2. First, the experimental set-up is described. In section 3.2, the *in vivo* orientation distribution and the mechanical properties of the collagen fibres in human skin are characterised, employing Lanir's Skin Model. Eventually, the method and model used for characterising the mechanical behaviour of human skin *in vivo* are discussed and conclusions are drawn.

3.1 Experimental Set-up

Field information of a piece of skin under investigation can be obtained by registering the positions of markers on its surface during deformation. For this purpose, a special measuring system has been developed. This measuring system is described in the next section. Information about the absolute stiffness can be obtained by measuring reaction forces required to deform the skin under investigation. In order to limit the deformation of the skin under investigation to a certain area, it is isolated from its surrounding area. The isolation of *in vivo* skin is explained in section 3.1.2.

3.1.1 Measuring System

In order to impose a certain state of deformation in the skin, a small surface tensile device is used. A schematic representation of the device is shown in figure 3.1. The pads ($6 \times 5\ mm^2$) of the device can be glued to the skin using cyanoacrylate resin. An electric motor drives the translating arms in opposite directions by means of a spindle. Using the measuring and controlling software Labview (National Instruments, 1992), the displacements of the pads can be prescribed in an arbitrary way. The displacement of the pads is registered with a Linear Variable Differential Transformer (LVDT) and the force on each pad is measured using strain gauged leaf springs. The accuracy of the measured force is 0.01 *N*. With Labview, the forces on the pads can be controlled. The prescribed displacement of the pads is automatically overruled, when the measured forces become too high for the strain gauged leaf springs. The prescribed displacement of the pads can also be overruled manually when the test person is in pain. In this way safety is build in during an experiment.

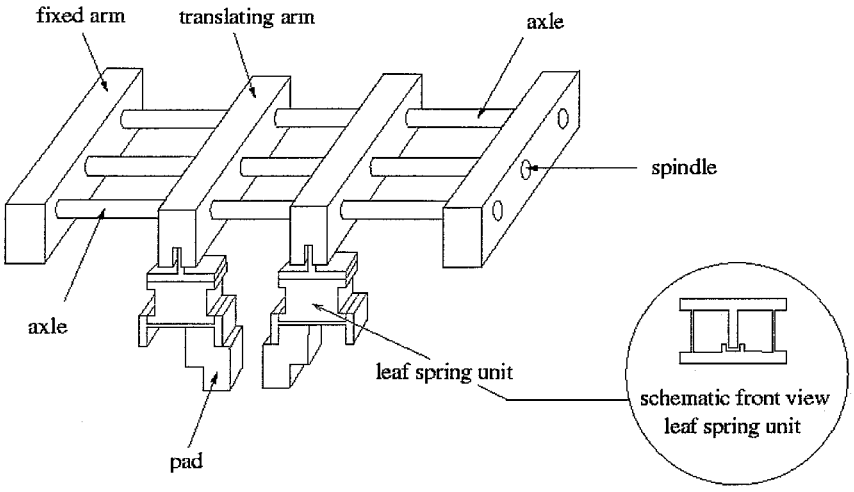

Figure 3.1: Schematic representation of the tensile device.

To obtain field information, a number of markers is applied to the surface of the skin. The size of the marker pattern is restricted to the dimensions of the tensile device. The number of markers and their diameter have been realised to meet several conflicting demands [Voorden, 1996]. Figure 3.3a shows the dimensions of the marker pattern. The marker pattern is applied to the skin under investigation by means of a template and using white oil paint (Royal Talens, titanium white).

The part of the body of a test person under investigation is positioned on a cushion of natural rubber, filled with small polystyrene spheres. This cushion can be sucked vacuum, providing a fixation of the part of the body resting in it, thus reducing movement to a minimum. Next, on each side of the marker pattern, the pads are glued to the skin. For characterisation of the in-plane mechanical behaviour of skin 2D measurements are most suitable. For this purpose, a CCD camera with a 105 *mm* lens is placed perpendicularly above the marker pattern. It is placed at a working distance of about 700 *mm*. With this CCD camera, connected to a super-VHS video recorder and an on-line video screen, the markers can be observed. In figure 3.2 a schematic representation is given of the measuring system during a tensile test on the arm of a test person.

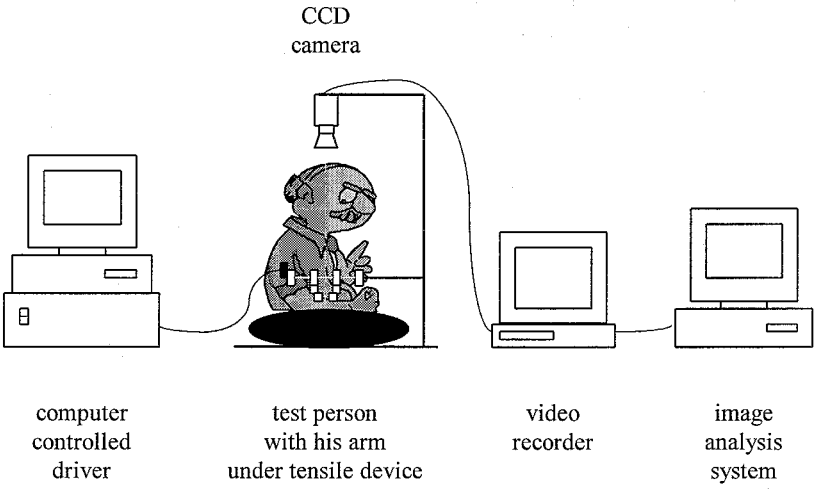

Figure 3.2: Schematic representation of the measuring system for *in vivo* experiments.

From the video recording images at different states of deformation are taken by a frame-grabber on a PC. The individual positions of the markers can be determined using the image analysis software Quantimet 500+ (Leica, 1994). The accuracy of the reconstructed marker positions proved to be 0.004 *mm* for the x-coordinate and 0.003 *mm* for the y-coordinate at a working distance of 580 *mm* [Voorden,1996]. The difference between the standard deviation in the x-direction and the y-direction is explained by the mechanical instability of the video tape which is known to be higher in the x-direction compared to the y-direction.

In order to generate strain distributions in a piece of skin, each marker position has to be followed in time. Therefore, the marker positions of successive states of deformation are matched [Peters, 1987]. For a minimal marker distance of 2 *mm* the positions of the markers can be matched, if the displacement of the pads between two successive states of deformation is equal or less than 2 *mm*.

3.1.2 Isolation of Skin

In order to limit the area of deformed skin under investigation, it is isolated from its surrounding area. For this purpose, a small plastic frame is designed, which can be glued to the skin. Figure 3.3b shows the design of the frame. The medial part of the frame is designed for the marker pattern to fit in. For a good attachment to the skin, the upper and the lower part are chosen round. The length of the area of skin enclosed by the frame is large enough to prevent that wrinkling of the skin behind the pads occurs. Stiffness of the frame is obtained by its thickness and height, which are both 3 *mm*.

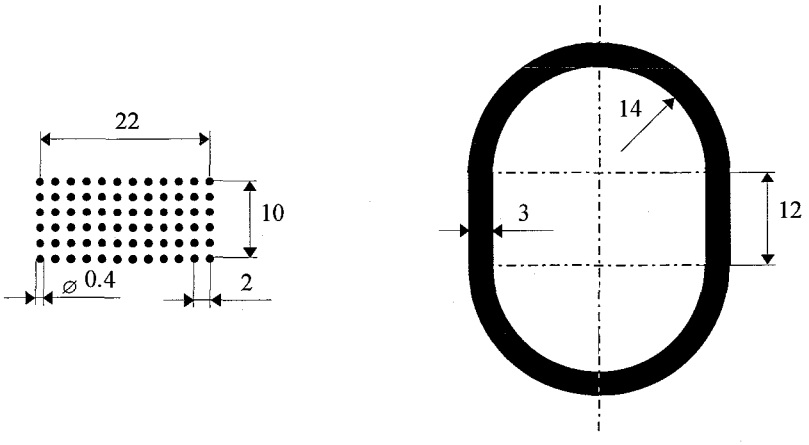

Figure 3.3: a) Design of the marker pattern. b) Design of the frame.
Sizes in *mm* (real size).

When the frame is glued to the skin, it will not only isolate a part of the skin from its surroudings, but it will also level the skin, which is extra convenient for 2D measurements. Figure 3.4 shows the marked skin isolated by the frame. The markers placed 10 *mm* from each other at each side of the frame are applied in order to position the frame almost symmetrical around the marker pattern on the skin. The other markers on the frame are applied in order to be able to reconstruct the position of the frame (see section 3.2.2). The dash-dotted lines in figure 3.4 represent the outlines of the camera view. The arrows at the pads point in the moving direction. Because it is hard to get the pads exactly straight into view, their displacements are reconstructed by registering the positions of the markers on the corners of the pads.

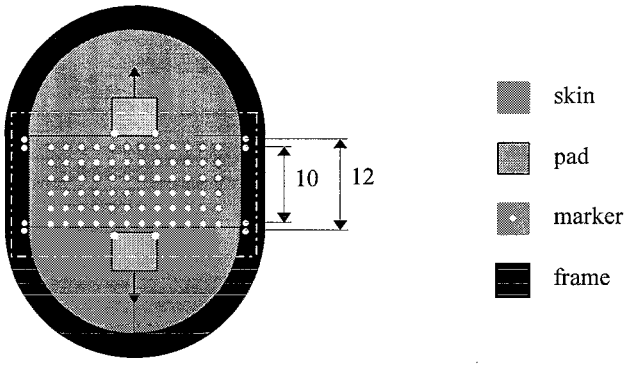

Figure 3.4: *In vivo* skin isolated from its surrounded area by a hard plastic frame.
The dash-dotted lines mark the camera view. The arrows point in the moving direction. Sizes in *mm*.

3.2 Mechanical Characterisation of Human Skin

For the characterisation of the mechanical behaviour of human skin, *in vivo* experiments are carried out. The performing of the experiments is outlined in the next section. Next, in section 3.2.2, a finite element model that is used to simulate the above mentioned experiment is described. In section 3.2.3, the constitutive model as it is used in the estimation process, is described and motivated. Eventually, some parameters of Lanir's Skin Model are estimated.

3.2.1 *In Vivo* Experiments

The optimal design of stretch tests for the structural characterisation of tissues requires two uniaxial stretch tests at mutually perpendicular directions inclined by 22.5° to the specimens axes of material symmetry [Lanir, 1996]. Since the direction of Langer's Lines coincides with the preferred orientation of collagen and elastin in the dermis, these lines give an indication of skin's axes of material symmetry [Langer, 1861], [Reihsner et al., 1994]. Therefore, two experiments are carried out: one at which the skin is stretched in the direction inclined by 22.5° to its Langer's Lines and one at a direction perpendicular to this.

Because of the 2D measurements, the skin under investigation is required to be flat. For the convenience of the test person, the best place to carry out the experiment is at the fore-arm. For characterisation of anisotropic mechanical behaviour, the collagen fibre distribution in skin is required to be anisotropic and homogeneous. To satisfy all these requirements, information about the anisotropy and inhomogenity of the mechanical behaviour of the skin at the arm was gathered. From Stark [Stark, 1977] and the distribution of Langer's Lines [Langer, 1861], the best place to carry out the experiments is at the inner side of the fore-arm near the elbow (see figure 1.3). The epidermis at the inner side of the arm is relatively thin. This is extra convenient for mechanical characterisation of the dermis. The death cells of the surface layer of the epidermis, the stratum cormeum, are relatively loosly connected to its underlying layers. They are removed by using scrub-cream, in order to enhance the attachment of the pads to the skin. Besides, the hydration of the stratum corneum will decrease its influence on skin's mechanical behaviour.

The marker pattern and the frame are applied at the inner side of the right fore-arm of a 33-year-old male person. The arm is fixed in such a position that the isolated piece of skin is perpendicular with respect to the camera. Next, the pads are glued to the surface of the skin as shown in the photograph of figure 3.5.

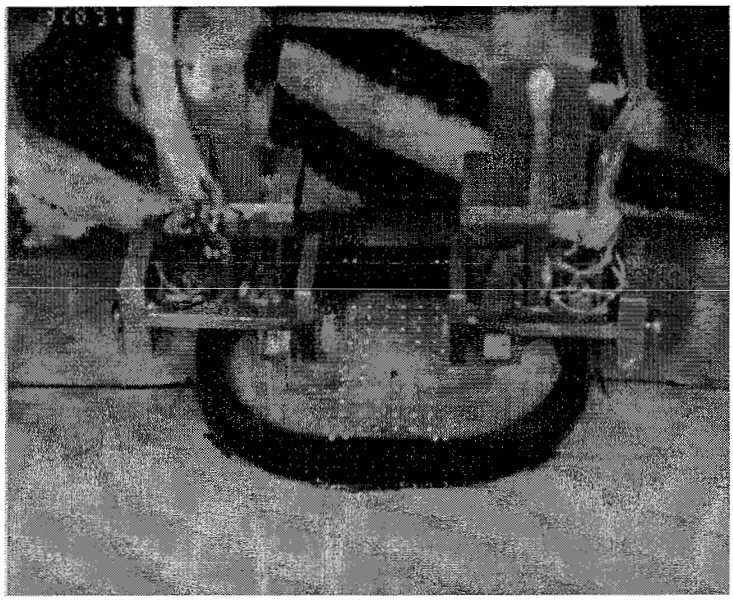

Figure 3.5: Photograph taken at the time the pads were glued to the skin.

In figure 3.6, the position of the frame and the direction of stretching is drawn schematically for both experiments. In the first experiment, the skin is stretched perpendicular to the direction inclined by approximately 22.5° to the direction of Langer's Line (see figure 3.6a). This experiment will further be called the transverse experiment, because the direction of stretching is about transverse to the long axis of the fore-arm. In the second experiment, called the longitudinal experiment, the frame and the direction of stretching are rotated by 90°(see figure 3.6b).

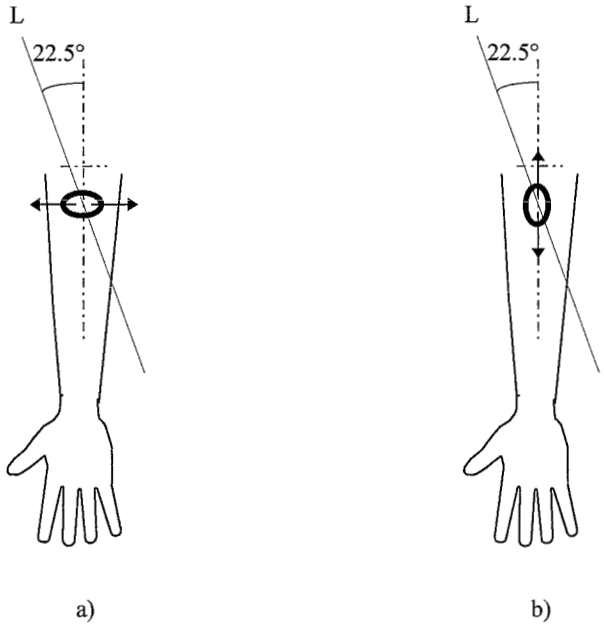

Figure 3.6: Positions of the frame at the inner side of the right fore-arm and directions of stretching. The line marked by the letter 'L' indicates the approximate direction of Langer's Lines.
a) Transverse experiment, b) Longitudinal experiment.

The initial distance between the pads is approximately 12.6 *mm*. In order to characterise the collagen fibre stiffness in skin, collagen fibres must get straightened and stretched. In the linear part of the stress-strain curve, as shown in stage III mentioned in figure 1.2, collagen fibres are straightened and stretched. In *in vitro* stretch tests on whole human skin, the beginning of the linear part of the stress-strain curve is reached at an extension of about 40% [Daly, 1966]. For anisotropic skin, the amount of extension at which the fibres are straightened and stretched varies for different directions. This is attributed to the reorientation of the fibres in the direction of the load. According to the approximate angles at which the skin is stretched with regard to the preferred direction of the collagen fibres, the linear part of the stress-strain curve for the transverse experiment will be obtained at a higher extension than for the longitudinal experiment.

From pilot experiments using pads with a surface of 10×5 mm^2 glued to the skin, it was observed that when the pads were moved 3 *mm* apart, reaction forces were too high for the strain gauged leaf springs. For this reason, pads with a surface of 6×5 mm^2 are used. They are moved as much as possible, being 4 *mm* in the transverse experiment and 3.5 *mm* in the longitudinal experiment. This is done in four steps with a constant velocity of 0.20 *mm/s*. After each step, the skin is given time to relax in order to measure the reaction force of the fibres and not the viscous part of the skin. The relaxation time needed increases with increasing load. Figure 3.7 shows the prescribed displacements of the pads and the measured reaction forces for both experiments. In figure 3.7b it can be seen that at the end of each relaxation period of the longitudinal experiment the skin is not fully relaxed. Because of the experiment carried out on a living human, longer relaxation periods are not recommended.

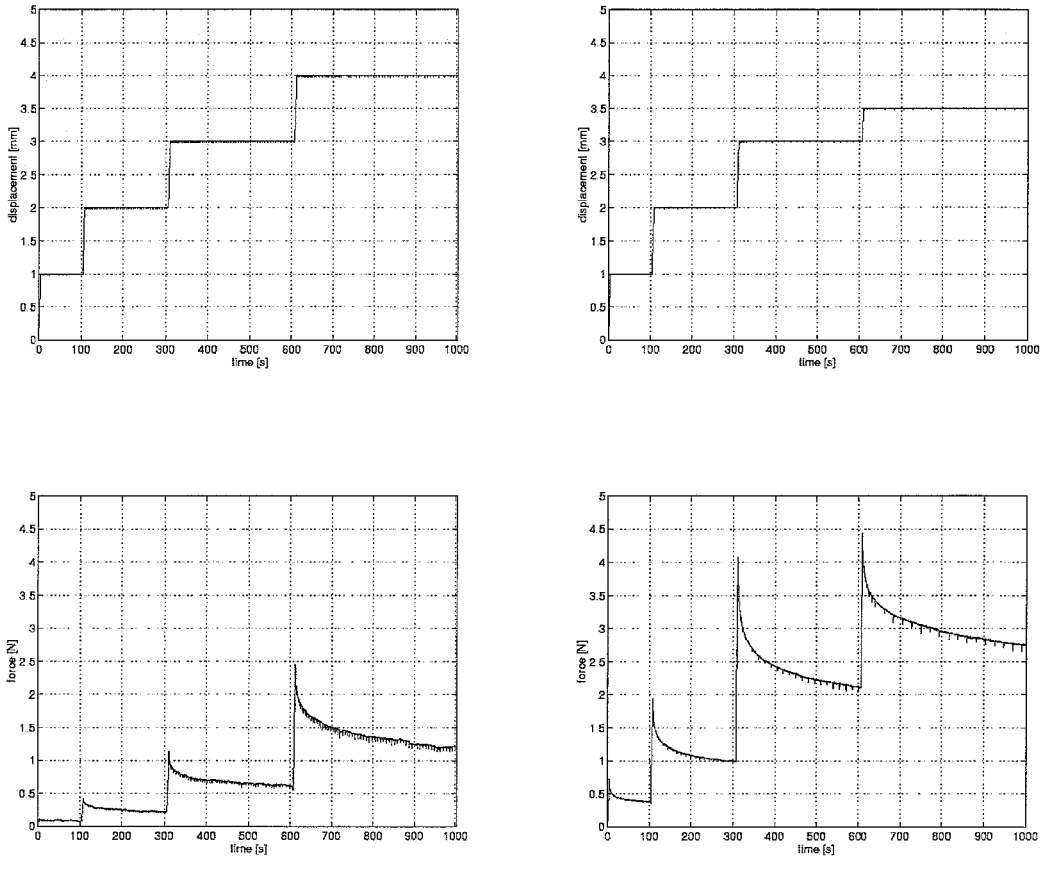

Figure 3.7: Prescribed displacements of the pads and mean measured reaction forces.
a) Transverse experiment, b) Longitudinal experiment.

The ambient conditions during the transverse experiment were measured to be 23.6 °C and 34% humidity. During the longitudinal experiment the ambient conditions were 22.4 °C and 32% humidity. These small differences in ambient conditions are assumed not to influence the mechanical behaviour of the skin under investigation significantly.

From the video recording, five pictures are taken. One at the starting point and four at the end of each relaxation period. Using the displacements of the eight makers on the frame (see figure 3.4), a correction of small movements of the test person can be made. The results of the corrections for small movements are shown in figure 3.8. The pictures at the top show the measured marker positions and the pictures below show the corrected marker positions. The markers at reference state are represented by 'o' and the displaced marker positions by ' × '.

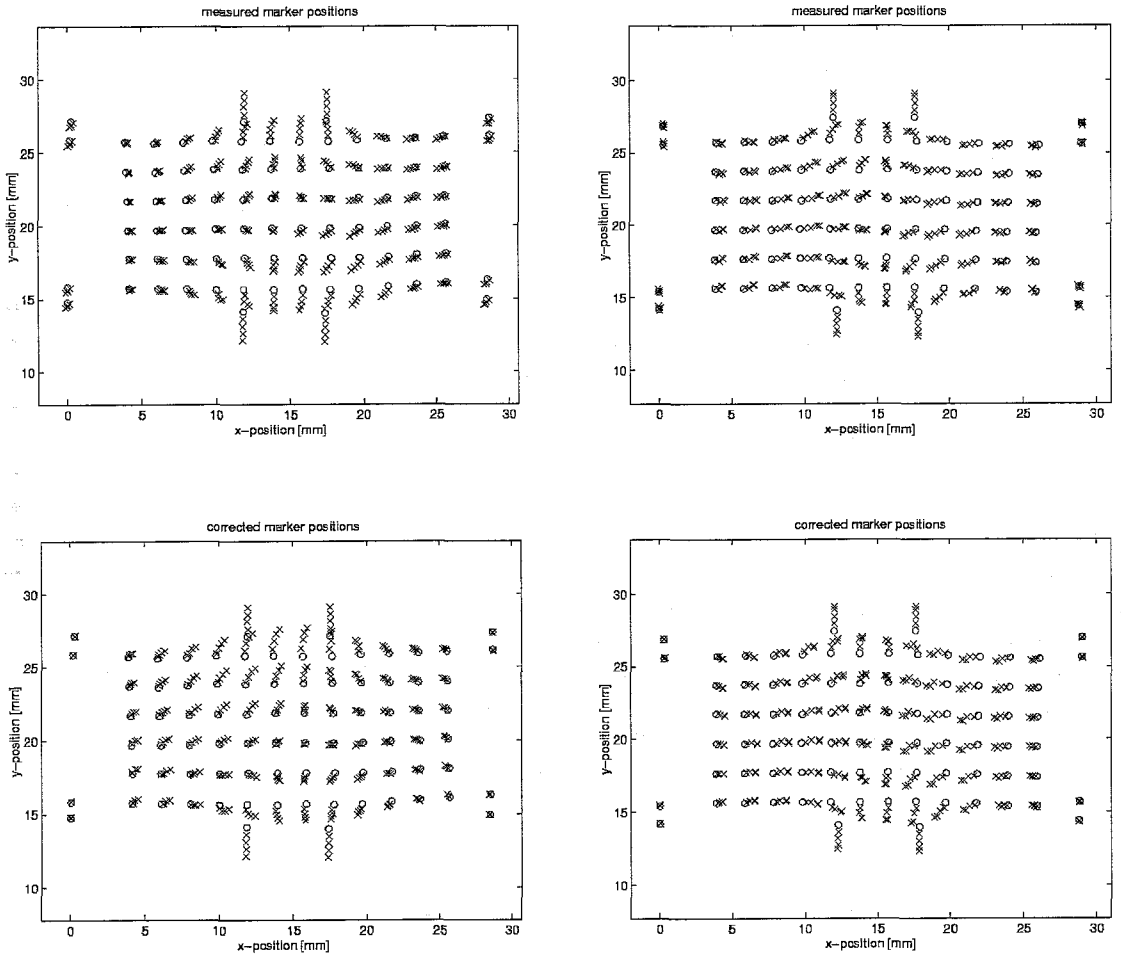

Figure 3.8: Results of the correction for small movements of the test person.
At the top: measured marker positions of different states of deformation. Under: the corrected marker positions. The marker positions of the reference state are represented by 'o' and the displaced marker positions by ' × '.
a) Transverse experiment, b) Longitudinal experiment.

Principal Green-Lagrange strain fields give an indication about the inhomogenity of a strain field. From the marker displacements Green-Lagrange strains of a certain state can be estimated with respect to the reference state [Ratingen, 1994], [Voorden, 1996]. Figure 3.9 shows the principal Green-Lagrange strain

fields of state 4 for both experiments. At every marker position at the skin, the principal strain is represented by two lines, where the solid lines represent positive principal strains and the dotted lines negative principal strains. The direction and the length of each line corresponds to the direction and the value of the local principal strain. It is seen that the principal strain field for the Transverse experiment is inhomogeneous. Therefore, it is assumed that this strain field contains enough information for the identification of a limited set of parameters. In the longitudinal experiment, the principal strains in the area between the pads differ significantly from those left and right from this area (see figure 3.9b).

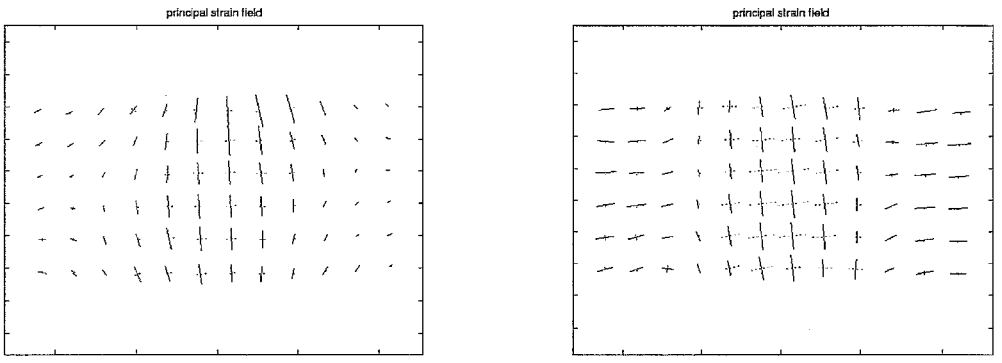

a) b)

Figure 3.9: Principal strain fields of deformation state 4.
The solid lines represent the positive strains and the dotted lines the negative strains.
a) Transverse experiment, b) Longitudinal experiment.

3.2.2 Finite Element Model

As the fibre distributions in skin as well as the experiments are assumed to be two-dimensional, a two-dimensional finite element model of each experiment is made. All the measured marker positions of the reference state become nodes in the finite element model. The inner geometry of the frame is reconstructed from positions of the markers placed 12 *mm* apart on each side of the frame (see figure 3.3 and 3.4). The reconstructed geometry of the frame defines the edge of the finite element model. The locations of the pads are reconstructed using the positions of the markers at the corners of the pads. The space without markers is divided in elements in a way that it matches with the nodes defined by the positions of the markers. The resulting finite element meshes of the reference state are shown in figure 3.10.

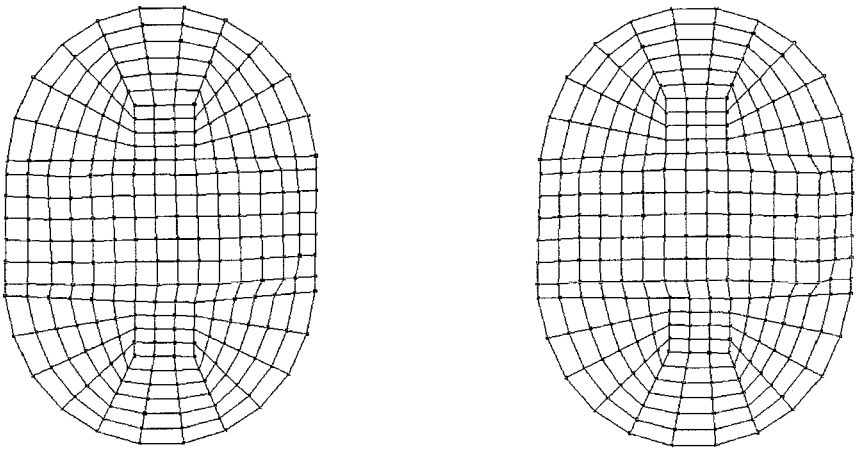

a) b)

Figure 3.10: Finite element meshes of the reference state.
a) Transverse experiment, b) Longitudinal experiment.

The pads and the frame are assumed to be infinitely stiff in comparison with the skin. The skin glued to the frame and the skin glued to the pads are assumed to be firmly tied. Therefore, it is modelled rigid. The edge of the finite element model, which is defined by the frame, is fixed. The measured displacements of the pads are prescribed to the rigid modelled skin under the pads. In figure 3.11, all the boundary conditions of the finite element model are shown. The displacements of the pads are represented by $\vec{u}_1$ and $\vec{u}_2$.

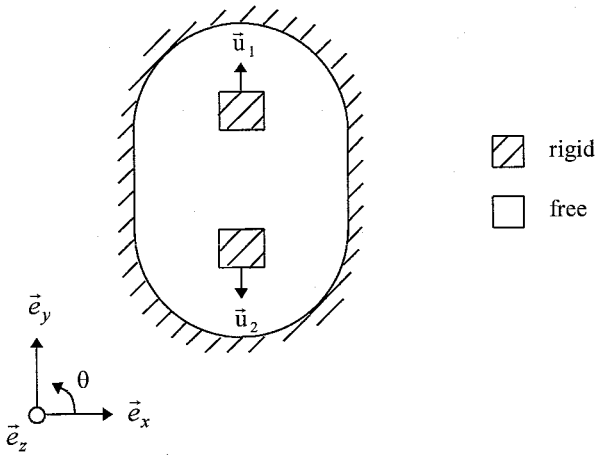

Figure 3.11: Boundary conditions of the finite element model.
The displacements of the pads are represented by $\vec{u}_1$ and $\vec{u}_2$.

Reaction forces of the skin are required to get information about the undulation and the stiffness of the fibres. The forces measured at each end of a relaxation period can be used in the estimation process. The reaction force of the skin during an experiment is only measured in the direction of its displacement. In the finite element model, the sum of the calculated nodal reaction forces in the y-direction of nodes corresponds to the y-component of the measured force on a pad. The deformed finite element meshes of state 4 are shown in figure 3.12.

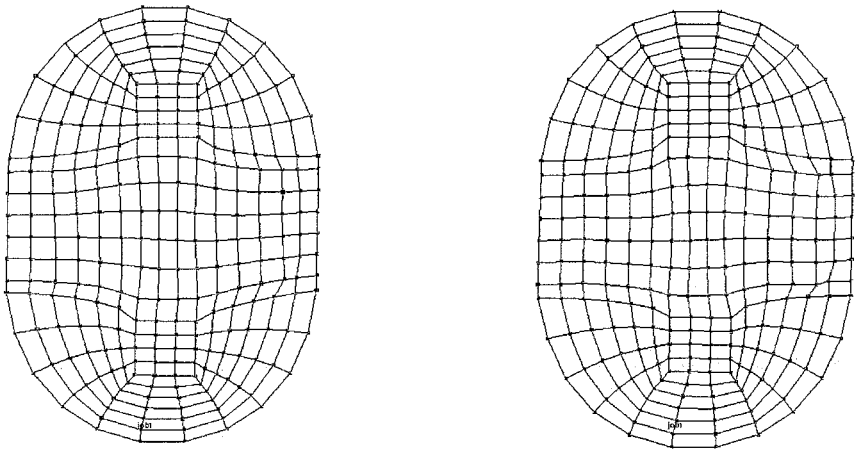

a) b)

Figure 3.12: Finite element meshes of deformation state 4.
a) Transverse experiment, b) Longitudinal experiment.

3.2.3 Parameters of Lanir's Skin Model

Lanir's Skin Model contains a lot of parameters. Because skin's mechanical behaviour is dominated by the collagen fibres in the dermis, only collagen parameters will be estimated. Since computing effort increases with the number of parameters, the set of estimated parameters has to be limited.

The fraction of collagen and elastin fibres in the skin, S_c and S_e respectively, are well determined in earlier research [Manschot, 1985]. Values for the stiffness of the collagen and elastin fibres, K_c and K_e respectively, are also known from literature, but the accuracy of the values is unknown. The mean undulation of collagen fibres, μ_c, is roughly guessed at about a quarter of its length [Manschot, 1985]. Its standard deviation, σ_c, is assumed to be the same as that of elastin. Elastin fibres in skin are assumed to be already strained. Therefore, the mean undulation of the elastin fibres, μ_e, equals 0 and its standard deviation, σ_e, is set to 0.2 (see section 2.1.4). The collagen fibre distribution is known to be preferably orientated in the direction of Langer's Lines [Langer, 1861]. The direction of Langer's Lines at the skin under investigation is approximately known, but exact values for the collagen fibre distribution are not known (see figures 1.3 and 3.6). In the collagen fibre orientation distribution function used in this research, defined by equation (2.6), parameter C_1 indicates the measure of anisotropy and C_2 the preferred orientation angle. The elastin fibres are assumed to be distributed isotropically. The numerical integration of the fibre orientation distribution functions is done with the trapezium rule using 24 intervals, so $\Delta\theta$ equals 7.5°.

Because of the incompressibility of skin, the finite element model needs stiffness in z-direction and an arbitrary thickness. When skin is deformed in-plane, the few collagen fibres which are directed perpendicularly to the plane are assumed to be compressed. Since fibres are assumed to have no compressive stiffness (see section 2.1.1), the collagen fibres will not contribute to the mechanical behaviour in the direction perpendicular to the skin. Therefore, the stiffness in this direction is assumed to be smaller than the in-plane stiffness of the skin. In the numerical model, the same values as for the fraction and stiffness of elastin in-plane are prescribed to the z-direction. From literature, the skin thickness at the inner fore-arm is measured to be 1.51 ± 0.07 *mm* [Reihsner et al., 1994]. The finite element model is given an arbitrary thickness of 1.51 *mm*.

From some finite element calculations, it was observed that variation of the stiffness of elastin, K_e, and the standard deviation of the mean undulation of collagen fibres, σ_c, do not influence the calculated reaction forces significantly. This confirms that the parameters to be estimated are the ones that dominate the mechanical behaviour of skin.

Summarising, the parameters of Lanir's Skin Model to be estimated are the collagen fibre stiffness, K_c, its mean undulation, μ_c, and the parameters defining the fibre orientation distribution, C_1 and C_2 according to equation (2.6). The assumed and expected values of the parameters of Lanir's Skin Model are given in table 3.1.

Parameter		Value	Dimension	Source
Fraction	S_c	0.30	-	Manschot, 1985
	S_e	0.02	-	
	S_z	0.02	-	
Stiffness	K_c	100	N/mm^2	Savenije, 1982
	K_e	1	N/mm^2	
	K_z	1	N/mm^2	
Undulation	μ_c	1.2-1.6$^{(*)}$	-	Manschot, 1985
	σ_c	0.2	-	
	μ_e	0	-	
	σ_e	0.2	-	
Orientation distribution of collagen	C_1	0.4-0.8$^{(*)}$	-	Reihsner et al., 1994
	C_2	0.40$^{(*T)}$	*rad*	
		1.96$^{(*L)}$	*rad*	
c: collagen in-plane		* : expected		
e: elastin in-plane		$*^T$: expected for Transverse experiment		
z: z-direction		$*^L$: expected for Longitudinal experiment		

Table 3.1: Parameters and their values of Lanir's Skin Model.

3.2.4 Parameter Estimation

For estimating all four parameters, the measured reaction forces as well as the marker displacements are used in the estimation process. The two kinds of experimental data differ in amount, value and dimension. Therefore, it is hard to determine appropriate values for their weight in the estimation process. In case the amount of data were weighted equal, estimation times were long and the estimation results were bad. So, more information about the influence of these four parameters on the reaction forces and the marker displacements is required. For this purpose, some numerical simulations are done, where the influence of each parameter on the calculated reaction forces and the marker positions is determined. Table 3.1 is used as indication for the range of variation of each parameter. The results of this analysis are shown in appendix B.

From the numerical simulations, it appears that the reaction forces are mainly characterised by the collagen stiffness, K_c, and particularly its mean undulation, μ_c (see figure B.1 and B.4). The marker displacements are mainly characterised by the collagen fibre orientation distribution parameters, C_1 and C_2, and by μ_c (see figures B.2, B.3, B.5 and B.6). The marker displacements are influenced by C_1 and C_2 in mutually perpendicular directions, while in most cases μ_c influences the marker displacements in almost the same direction as that of C_1. The influence of K_c on the marker displacements can be neglected. So, C_1 and C_2 can only be estimated from the marker displacements, if μ_c is known. It is expected that a rough estimate for μ_c can be made, using the measured reaction forces. K_c can be

estimated based on the reaction forces only. The estimation sequence used in order to get a good estimation of all four parameters is now described below.

First, K_c and μ_c are estimated using the measured reaction forces on each pad at the end of each relaxation period. Using the experimental data of successive states of deformation in each estimation step has proven to be effective [Starmans, 1994]. The measured forces at each pad of all four states of deformation are collected in one single observation column of dimension 8×1 defined as:

$$\underset{\sim f}{y} = \left[(f_1)_1, (f_2)_1, \ldots\ldots, (f_1)_4, (f_2)_4\right]^T \tag{3.1}$$

Next, C_1 and C_2 are estimated using the measured marker coordinates of each state of deformation, and using the last estimated values for K_c and μ_c. All the measured marker coordinates are collected in one observation column of dimension 572×1 defined as:

$$\underset{\sim xy}{y} = \left[(x_1)_1, (y_1)_1, \ldots, (x_{144})_1, (y_{144})_1, \ldots\ldots, (x_1)_4, (y_1)_4, \ldots, (x_{144})_4, (y_{144})_4\right]^T \tag{3.2}$$

This two-step estimation cycle is repeated until convergence of the parameters is reached. Because of excessive computation times, the number of estimation cycles is limited to two. The two-step estimation cycle is schematically presented in figure 3.13.

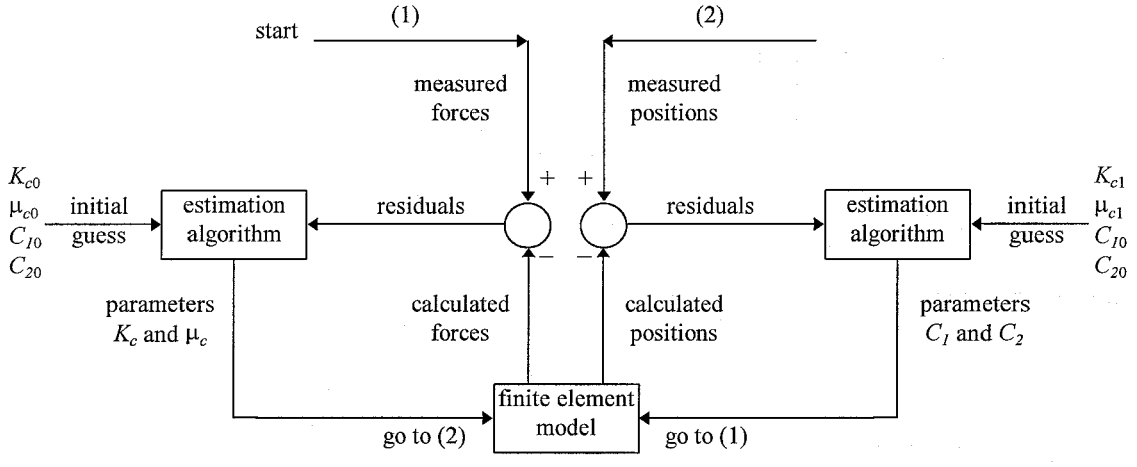

Figure 3.13: Diagram for the two-step estimation cycle.

To initialise the estimation sequence, an initial guess for the parameters to be estimated and an initial guess for the parameter covariances is needed. The parameters of each set are considered to be mutually independent. The accuracy of the experimental data and the confidence in the model are also taken into account (see appendix A). They are both considered to be mutually independent. The various standard deviations have a more or less physical meaning. However, it may also be advantageous to choose their values based on convergence considerations [Voorden, 1996].

The columns of parameters to be estimated are defined by:

$$\underset{\sim f}{x} = \left[K_c/100 \quad \mu_c\right]^T \qquad \text{and} \qquad \underset{\sim xy}{x} = \left[C_1 \quad C_2\right]^T \tag{3.3}$$

For numerical reasons the parameter K_c is scaled in the estimation process, by dividing its value by 100. The initial guesses for the parameters for the Transverse experiment are set to:

$$\underset{\sim f0}{\hat{x}} = \left[0.5 \quad 1.5\right]^T \qquad \text{and} \qquad \underset{\sim xy0}{\hat{x}} = \left[0.4 \quad 0.2\right]^T \tag{3.4}$$

In an attempt to exclude convergence to a local minimum, the estimation process is repeated for another set of initial guesses:

$$\underset{\sim f0}{\hat{x}} = [1.5 \quad 1.3]^T \qquad \text{and} \qquad \underset{\sim xy0}{\hat{x}} = [0.8 \quad 0.6]^T \tag{3.5}$$

The values of the initial guesses are based on table 3.1 and information from appendix B. An estimation process starting with the initial guesses stated in (3.4) will be called Case I, and with the initial guesses stated in (3.5) Case II. The chosen values for the initial guesses for the parameters C_1 and C_2 in each case have opposite influence on the reaction forces in the finite element model (see appendix B). In this way the first parameters to be estimated, K_c and μ_c, will be characterised better. A good first estimation of μ_c is very important for the estimation of the parameters C_1 and C_2.

For physical and numerical reasons, the constraints for the different parameters are set to:

$$\begin{aligned} &0.001 \le K_c/100 \le 2.000 \\ &1.100 \le \mu_c \le 1.700 \\ &0.001 \le C_1 \le 0.848 \\ &0.001 \le C_2 \le 3.141 \end{aligned} \tag{3.6}$$

The initial standard deviations of the parameters to be estimated are set to $2 \cdot 10^{-1}$. The standard deviations of all the experimental data are set to $1 \cdot 10^{-4}$ and the model standard deviations are set to $1 \cdot 10^{-2}$.

An extra advantage of estimating two columns of two parameters each, in stead of one column of four parameters, is that the total number of iterations needed will be less. This is due to the fact that less combinations of solutions for the parameters are possible. As stated before, the computing effort is still high. Therefore, the two-step estimation cycle is stopped after two estimations. The remainder of this section is divided into three parts. First the accuracy by which parameters can be estimated in two cycles is determined, next the estimation results of the Transverse experiment and the Longitudinal experiment are described.

Accuracy of the Estimated Parameters

In this section, an indication of the accuracy by which parameters can be estimated in two cycles is determined. Here, the Transverse experiment is simulated using a given set of parameters. The true values of the parameters are to be estimated in Case I and Case II. Their values, stated in table 3.2, are exactly between the initial guesses of Case I and Case II. For the generation of 'experimental' data, the finite element model of the Transverse experiment is used.

Parameter	True Value	Dimension
$K_c/100$	1.0	$N/mm^2/100$
μ_c	1.4	-
C_1	0.6	-
C_2	0.4	*rad*

Table 3.2: Given set of parameters of the simulated Transverse experiment.

The 'experimental' data are generated using 60 intervals in the numerical integration of the fibre orientation distribution functions. The generated data are provided with random normal distributed noise. The standard deviation of the noise added to the generated reaction forces is 0.010 N and of the noise added to the generated marker coordinates is 0.005 *mm*.

The estimation sequence of the four parameters for both sets of initial guesses is shown in figure 3.14. The estimated parameter values are represented by solid lines and their true values by dotted lines. From this figure, it can be observed that in Case I the parameters μ_c, C_1 and C_2, are converged and that in Case II only μ_c is converged. From the estimated parameter values of both estimation steps, the other parameters are expected to be converged, if one or more estimations will be done.

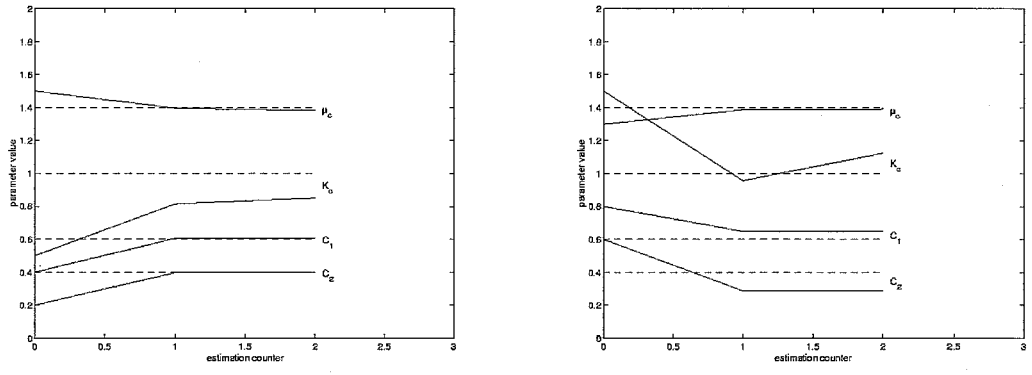

a) b)

Figure 3.14: Estimation sequence of the simulated experiment.
The estimated parameter values are represented by solid lines and their true values by dotted lines.
a) Estimation sequence of Case I, b) estimation sequence of Case II.

In order to assess estimation results, the measure χ_k^2 is introduced. This measure is defined by:

$$\chi_k^2 = (\underset{\sim k}{y} - \underset{\sim k}{h}(\underset{\sim k}{\hat{x}}))^T \underline{R}_k^{-1} (\underset{\sim k}{y} - \underset{\sim k}{h}(\underset{\sim k}{\hat{x}})), \tag{3.7}$$

where k is the estimation step and $\underline{R}_k^{-1}$ the diagonal matrix containing the standard deviations of the experimental data.

The estimation results of the simulated experiment for two different initial guesses are summarised in table 3.3. It can be observed that Case I results in a better estimation of parameters C_1 and C_2 compared to Case II, and Case II results in a better estimation of the parameters K_c and μ_c. The difference in the estimation results can be attributed to the speed of convergence being dependent on the initial guesses.

Parameter	Dimension	Case I			Case II		
		Intitial guess	Estimate 2nd	χ^2	Intitial guess	Estimate 2nd	χ^2
$K_c/100$	$N/mm^2/100$	0.5	0.849	$5.145 \cdot 10^5$	1.5	1.124	$3.633 \cdot 10^5$
μ_c	-	1.5	1.383		1.3	1.392	
C_1	-	0.4	0.603	$1.977 \cdot 10^6$	0.8	0.648	$2.993 \cdot 10^7$
C_2	*rad*	0.2	0.399		0.6	0.290	

Table 3.3: Estimation results of the simulated experiment.

The difference between experimental and calculated data, the residuals, can give an indication of the reliability of the parameters and the constitutive model employed. For easy interpretation of the residuals, the column of residuals is defined by:

$$\underset{\sim}{r} = \underset{\sim}{h}(\underset{\sim}{\hat{x}}) - \underset{\sim}{y}. \tag{3.8}$$

All residuals are calculated using the final estimates of Case I and Case II. In case of residual reaction forces, a positive value implies a positive deviation of the absolute value of the calculated reaction force compared to the measured reaction force. In case of the residual marker positions, a positive value implies a deviation of the calculated position compared to the measured position in positive x- or y-direction. The sample mean of the residuals of the reaction forces is the mean deviation of the reaction forces of both pads. In the ideal case of no modelling errors, the mean residual reaction force per state of deformation is in the order of magnitude of the measuring error. The sample mean of the residuals of the marker positions equals the mean orientation of the residuals. In the ideal case of no modelling errors, the distribution of the residual field should be random, and the order of magnitude of the residuals should be equal to the measuring error.

The residual marker positions of the last state of deformation of the simulated experiment is shown in figure 3.15. The measured positions of the markers are represented by 'o' and the calculated positions by '+'. To clarify the pictures, the residuals are multiplied by a factor 100 for Case I and by a factor 50 for Case II. It can be seen that the residuals of the marker positions are randomly distributed for Case I and exhibit some structure for Case II.

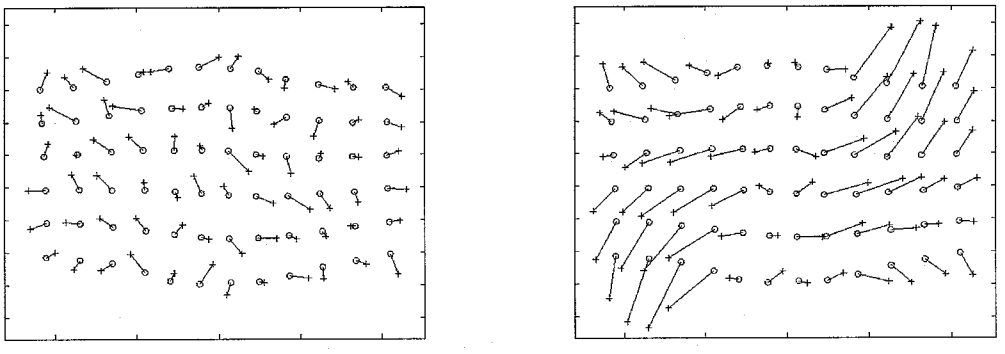

a) b)

Figure 3.15: Residuals of the marker positions for deformation state 4 of the simulated experiment. The measured markers positions are represented by 'o' and the calculated positions by '+'. a) Case I: multiplied by 100, b) Case II: multiplied by 50.

For more information about the possible modelling errors, the size and the structure of the residuals are evaluated. From the reaction forces the sample mean, $\bar{r}_f$, for each state of deformation is determined. From the residual marker positions, the sample means and the standard deviations of each deformation state for the x- and y-direction are determined, respectively indicated by $\bar{r}_x$, $\bar{r}_y$, s_x and s_y.

The residuals for the two cases of the simulated experiment are summarised in table 3.3. From this table, it can be observed that the mean residual reaction forces are in the order of magnitude of the added noise to the generated reaction forces. Although parameter K_c is characterised the worst, its deviation does not contribute to modelling errors significantly. A possible explanation for this, is that K_c can only be characterised accurately, if all collagen fibres are stretched. With a mean collagen fibre undulation of 1.4 a global stretch of about 40% is needed to get this situation. In the Transverse experiment, the pads are moved from 12.6 *mm* to 16.6 *mm* which does not result in a global stretch of 40% in the skin.

From table 3.4 it can also be observed that the standard deviations of the residual marker positions increases with increasing load. In Case I of the table, it can also be observed that, the standard deviation of the residual marker positions are not significantly higher than the standard deviation of the added noise to the generated 'experimental' data. Considering its random distribution, it can be stated that the estimation of the parameters C_1 and C_2 is converged in Case I. It can be stated that the modelling error created by using 24 intervals in the numerical integration of the fibre orientation distribution functions is not relevant (60 intervals were used for the generation of data). The standard deviations of the marker positions in Case I are lower than in Case II.

State	Case I					Case II				
	[N]	[mm]	[mm]	[mm]	[mm]	[N]	[mm]	[mm]	[mm]	[mm]
1	0.0078	0.0005	0.0055	0.0002	0.0052	0.0147	-0.0003	0.0106	0.0004	0.0099
2	0.0049	0.0001	0.0057	0.0005	0.0055	0.0226	0.0000	0.0187	0.0011	0.0181
3	-0.0041	0.0002	0.0057	0.0002	0.0056	0.0290	-0.0004	0.0259	0.0010	0.0240
4	-0.0311	0.0006	0.0074	0.0005	0.0063	0.0296	0.0004	0.0326	0.0015	0.0318

Table 3.4: Sample means and standard deviations of the residuals of the simulated experiment.

Summarising, it can be stated that, using two different intial guesses defined in equations (3.4) and (3.5) respectively, it is possible to get a converged solution for a set of parameters in two estimation cycles. The accuracy by which the parameters μ_c, C_1 and C_2 can be estimated is about $1 \cdot 10^{-2}$. The parameter K_c cannot be estimated accurately, but its deviation does not contribute to modelling errors significantly. Using 24 intervals in the numerical integration of the fibre orientation distribution functions does not lead to modelling errors significantly either.

Estimation Results of the Transverse Experiment

The estimation sequence of the four parameters for both sets of initial guesses for the Transverse experiment is shown in figure 3.16. To clarify the picture, the estimation sequence of parameter K_c is represented by dotted lines. From the figure, it can be observed that all parameters except K_c are converged. This parameter is expected to increase with more estimations, as a third estimation in one of the Cases showed an increase.

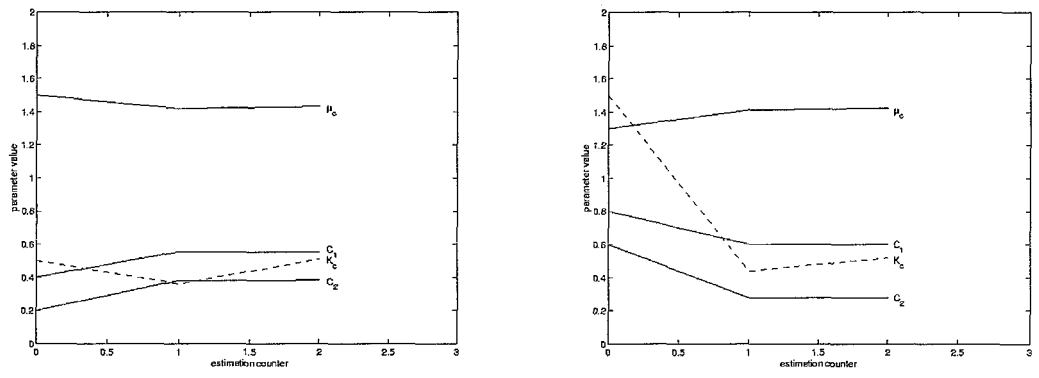

a) b)

Figure 3.16: Estimation sequence of the Transverse experiment.
a) Estimation sequence of Case I, b) estimation sequence of Case II.

The estimation results of the Transverse experiment of the two Cases are summarised in table 3.5. From the values for χ^2, it can be observed that the estimation of Case I results in a slightly better estimation for both columns of parameters. It can also be observed that χ^2 of the estimation results of K_c and μ_c are one order of magnitude higher than the expected minimal values in table 3.3, and that χ^2 of the estimation results C_1 and C_2 is three orders of magnitude higher. The estimated parameters correspond to their expected values (see table 3.1).

Parameter	Dimension	Case I			Case II		
		Intitial guess	Estimate 2nd	χ^2	Intitial guess	Estimate 2nd	χ^2
$K_c/100$	$N/mm^2/100$	0.5	0.509		1.5	0.518	
μ_c	-	1.5	1.433	$5.156 \cdot 10^6$	1.3	1.425	$5.233 \cdot 10^6$
C_1	-	0.4	0.552		0.8	0.599	
C_2	*rad*	0.2	0.382	$1.308 \cdot 10^9$	0.6	0.279	$1.330 \cdot 10^9$

Table 3.5: Estimation results of the Transverse experiment.

The residuals for the two cases of the Transverse experiment are summarised in table 3.6. From this table, it can be observed that the mean residual reaction forces are in the order of magnitude of the accuracy of the leaf springs, except for state 2.

From table 3.6, it can also be observed that the standard deviations of the residual marker positions increase with increasing load just like in the simulated experiment. The standard deviations are about an order of magnitude larger than expected. Little difference is seen in the residuals of both cases. This confirms that the solution (estimates) for the parameters is converged.

State	Case I					Case II				
	[N]	[mm]	[mm]	[mm]	[mm]	[N]	[mm]	[mm]	[mm]	[mm]
1	0.0409	0.0365	0.0644	-0.0139	0.0543	0.0455	0.0358	0.0581	-0.0137	0.0525
2	0.1112	0.0014	0.0699	-0.0931	0.0666	0.1192	0.0013	0.0565	-0.0926	0.0644
3	0.0479	-0.0209	0.0597	-0.2150	0.0742	0.0538	-0.0215	0.0563	-0.2143	0.0784
4	-0.0618	-0.0960	0.1067	-0.2476	0.1346	-0.0688	-0.0963	0.1208	-0.2467	0.1468

Table 3.6: Sample means and standard deviations of the residuals of the Transverse experiment.

The residual marker positions for Case I of all states of deformation of the Transverse experiment are shown in figure 3.17. The measured positions of the markers are represented by 'o' and the calculated positions by '+'. To clarify the pictures, the residuals are multiplied by a factor 5. It can be seen that the residuals of the marker positions of all states of deformation are not orientated randomly, but exhibit structure. For Case II the structure is the same. The structure and the size of the residuals indicate the presence of modelling errors.

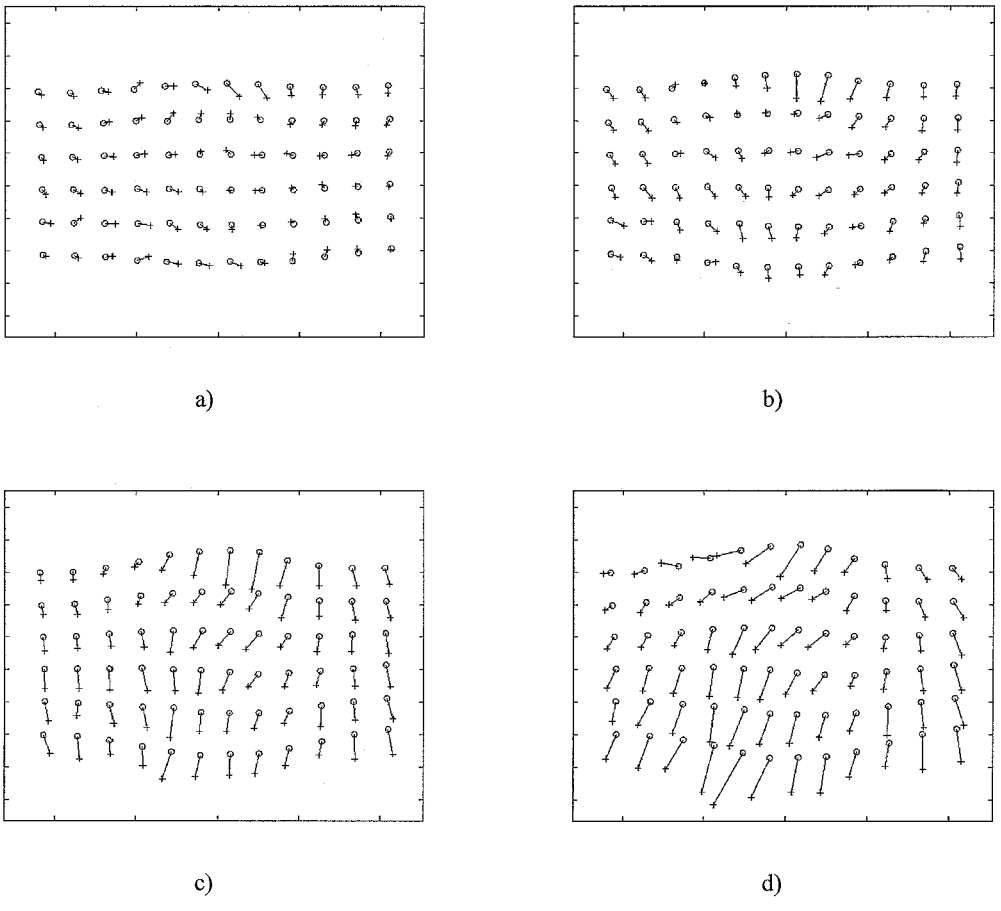

Figure 3.17: Residuals of the marker positions of different states of deformation of the Transverse experiment. The measured markers positions are represented by 'o' and the calculated positions by '+'. a) State 1, b) state 2, c) state 3 and d) state 4. The residuals are all multiplied by a factor 5.

Estimation Results of the Longitudial Experiment

The Longitudinal experiment is used for the verification of the estimated parameters of the Transverse experiment. However, during the estimations of the parameters, C_1 and C_2 were forced on their constraints. Considering the principal strain field obtained for the Longitudinal experiment (see figure 3.9b), the large differences of the principle strains may be the cause for these identification problems. For this reason, only the parameters K_c and μ_c of the Longitudinal experiment are estimated.

The Longitudinal experiment was carried out on the same piece of skin as the Transverse experiment, but the direction of loading was inclined by 90°. For this reason, it is assumed that the collagen fibre distribution is the same for both experiments and its preferred orientation is rotated by 90°. Because, in the Transverse experiment in Case I the residuals are smaller than in Case II, the values for the parameters C_1 and C_2 of Case I are used in the Longitudinal experiment. Thus, the value for fibre distribution parameter, C_1, is set to 0.552 and the preferred orientation angle, C_2, is set to 1.953 (0.382 + $\pi/2$). The estimation sequence of the parameters K_c and μ_c for both sets of initial guesses is shown in figure 3.18. From this figure, it can be seen that the parameters are almost converged.

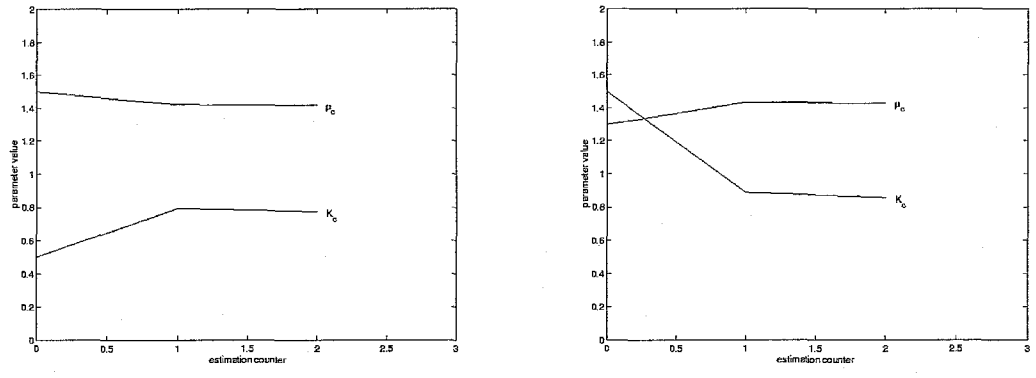

a) b)

Figure 3.18: Estimation sequence of the Longitudinal experiment.
a) Estimation sequence of Case I, b) estimation sequence of Case II.

The estimation results of the Longitudinal experiment for two different initial guesses are summarised in table 3.7. From the values for χ^2, it can be observed that Case II results in a slightly better estimation for the parameters K_c and μ_c compared to Case I. The estimated values for μ_c do not differ significantly from the estimated values for μ_c in the Transverse experiment. The estimated values for parameter K_c are higher than the values in the Transverse experiment. Although, in the Transverse experiment in case of more estimations, an increase of this parameter is expected.

Parameter	Dimension	Case I			Case II		
		Intitial guess	Estimate 2nd	χ^2	Intitial guess	Estimate 2nd	χ^2
$K_c/100$	$N/mm^2/100$	0.5	0.774	$3.966 \cdot 10^6$	1.5	0.857	$3.361 \cdot 10^6$
μ_c	-	1.5	1.418		1.3	1.429	

Table 3.7: Estimation results of the Longitudinal experiment.

For information about the modelling errors, the residuals for the two cases of the Longitudinal experiment are summarised in table 3.8. From this table, it can be observed that the mean residual reaction forces are in the order of magnitude of the measuring error of the leaf springs and are smaller than those of the Transverse experiment.

From table 3.8, it can also be observed that the standard deviations of the residual marker positions again increase with increasing load. The standard deviations are more than an order of magnitude larger than expected. Little difference is seen between the residuals of both cases.

State	Case I					Case II				
	$\bar{\cdot}_f$ [N]	$\bar{\cdot}$ [mm]	[mm]	$\bar{\cdot}$ [mm]	$\cdot_y$ [mm]	$\bar{\cdot}_f$ [N]	$\bar{\cdot}$ [mm]	[mm]	$\bar{\cdot}$ [mm]	$\cdot_y$ [mm]
1	-0.0223	0.0088	0.0524	0.0195	0.0945	-0.0285	0.0088	0.0524	0.0195	0.0944
2	-0.0126	0.0642	0.1918	-0.0568	0.1626	-0.0228	0.0623	0.1913	-0.0568	0.1623
3	-0.0632	-0.0415	0.3459	0.1369	0.2807	-0.0680	-0.0415	0.3449	0.1369	0.2801
4	0.0559	0.0581	0.3831	0.0699	0.3395	0.0618	0.0580	0.3818	0.0699	0.3388

Table 3.8: Sample means and standard deviations of the residuals of the Longitudinal experiment.

The residuals for Case II of the Longitudinal experiment are shown in figure 3.19. In figure 3.19a, the mean measured and calculated reaction forces are shown. The mean measured reaction forces are represented by solid lines and the mean calculated reaction forces by dotted lines. The residual marker positions of deformation state 4 is shown in figure 3.19b. Again, the measured positions of the markers are represented by 'o' and the calculated positions by '+'. To clarify the picture, the residuals of the marker positions are multiplied by a factor 5. It can be seen that the residuals of the marker positions exhibit structure. For Case I the structure is the same. The structure is totally different from the structure for the Transverse experiment (see figure 3.17). Again, the structure and the size of the residuals indicate the presence of modelling errors.

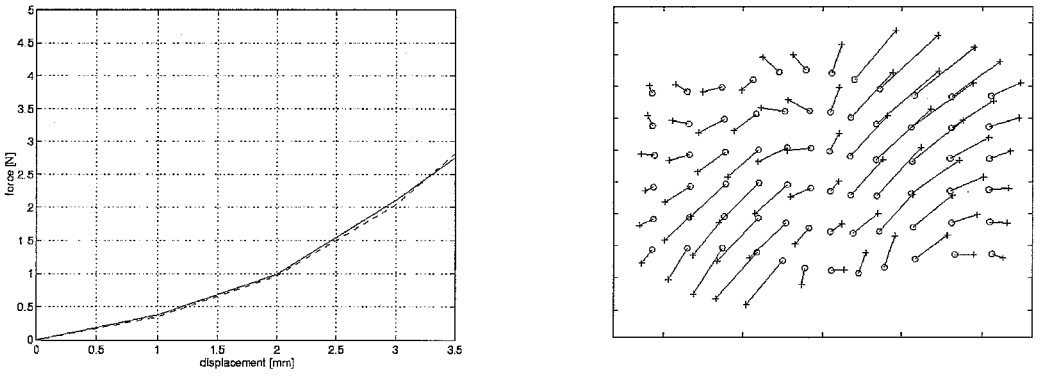

a) b)

Figure 3.19: Residuals for Case II of the Longitudinal experiment.
a) Mean measured forces (solid lines) and mean calculated forces (dotted lines).
b) Residuals of the marker positions of deformation state 4, multiplied by a factor 5.
The measured markers positions are represented by 'o' and the calculated positions by '+'.

3.3 Discussion & Conclusions

In this chapter the mechanical behaviour of human skin *in vivo* was characterised, employing a structural model. For this purpose, two experiments were carried out on one isolated piece of skin at the inner side of the fore-arm. In the first experiment, called the Transverse experiment, the direction of stretching was about transverse to the long axis of the fore-arm. In the second experiment, called the Longitudinal experiment, the direction of stretching was rotated by 90°. During the experiments, reaction forces of the skin and the marker positions of four states of deformation were measured. The measured reaction forces of the skin were used for the characterisation of the collagen fibre stiffness, K_c, and its mean undulation, μ_c. The marker positions were used for the characterisation of parameters describing the collagen fibre orientation distribution in the reference state C_1 and C_2. To exclude convergence to a local minimum, two different sets of initial guesses were used.

Evaluation of the estimation results leads to the following conclusions:

- From simulated 'experiments' it appears that the estimation process used is successful for both sets of initial guesses, but the speed of convergence differs.
- Using the data of the Transverse experiment, the same values are found for the estimated parameters starting from different initial guesses. All estimated values are in the expected range. For these reasons, the values become more reliable.
- Using the data of the Longitudinal experiment, it is only possible to characterise the collagen fibre stiffness and mean undulation. Using the estimated values for the parameters describing the collagen fibre orientation distribution of the Transverse experiment, it was possible to estimate the collagen fibre mean undulation and the collagen fibre stiffness.
- The residuals of the reaction forces are in the expected order of magnitude. The lowest residuals are found for the Longitudinal experiment. Resulting from all the estimations, the collagen fibre mean undulation, μ_c, ranges from 1.42 to 1.43 and the collagen fibre stiffness, K_c, from 50 to 90 N/mm^2. The estimated values for the collagen fibre stiffness do not differ significantly from values of earlier research [Savenije, 1984].
- The residuals of the marker positions are an order of magnitude larger than expected and exhibit structure, rather than randomness. The lowest residuals are calculated for the Transverse experiment. The structure for both experiments differs significantly. Further, the residuals of the marker positions increase with increasing load.

Summarising, it can be stated that the constitutive model used for the characterisation of the mechanical behaviour of human skin *in vivo* exhibits modelling errors. Below, a number of possible modelling errors are listed:

- Lanir's Skin Model is restricted to the characterisation of the dermis; the influence of the epidermis and hypodermis are neglected.
- The assumption that the epidermis moves exactly the same as the dermis upon deformation.
- The assumption that the collagen fibre orientation distribution in skin is flat.
- The fact that the skin was not fully relaxed during the Longitudinal experiment at the time the marker positions were measured.
- Lanir's Skin Model may have invalid assumptions.
- The assumption that the mechanical properties within the modelled area are homogeneous.
- The assumption that the measured skin surface is perfectly flat.

Chapter 4

Collagen Fibre Orientation in Skin during Deformation

In this chapter, information is gained about the in-plane collagen fibre orientation during deformation of *in vitro* skin. For this pupose, the optical technique Small Angle Light Scattering (SALS) as described in section 2.3 is used. First, the experimental set-up is described. In section 4.2, fibre orientations are derived from SALS measurements using Lanir's fibre density function (see section 2.1.3). Finally, the results are discussed and conclusions are drawn.

4.1 Experimental Set-up

Information about the collagen fibre orientation during deformation can be obtained by measuring the intensity pattern of the laser light diffracted by an *in vitro* piece of skin at different states of deformation. For this purpose, a measuring system is designed which is described in the next section. In order to obtain a bright image of the intensity pattern, the *in vitro* piece of skin under investigation needs some preparation. The preparation of *in vitro* skin is described in section 4.1.2.

4.1.1 Measuring System

To impose a certain state of deformation, a small tensile device is designed. A schematic representation of the tensile device is shown in figure 4.1. An isolated piece of skin can be fixed between the serrated jaws. These serrated jaws prevent slipping of the skin when it is stretched. By rotating the spindle manually, the skin can be stretched uniaxially from 10 to 14 *mm*. The hole in the tensile device will let the laser beam pass through uninterrupted.

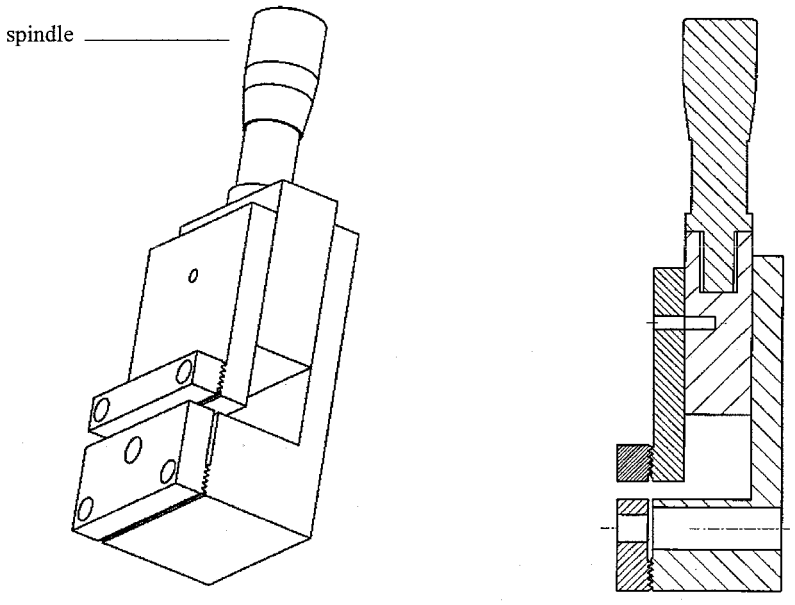

Figure 4.1: Schematic representation of the tensile device.
a) 3D representation, b) vertical cross section.

The SALS device used consists of an unpolarised Helium-Neon laser (6 *mW* at 633 *nm* wavelength) mounted on an optical table, along with a beam expander, a positioner for the tensile device and detection equipment. A schematic representation of the SALS measuring system is shown in figure 4.2. The beam expander, consisting of two convex lenses and three diaphragms, enlarges the diameter of the laser beam from 1 to 3 *mm*. Beam expansion is required to minimise the effect of local irregularities in the specimen by measuring over a larger area. The tensile device is placed in a special positioner, in order to position the plane of the specimen perpendicular to the optical axis (laser beam). The detection equipment consists of a black & white CCD camera connected to a PC equiped with a frame grabber. From the CCD camera, the intensity distribution images of different states of deformation are saved. CCD cameras saturate very easily, requiring the laser light to be significantly attenuated prior to reaching the camera. Because only the diffracted laser light is relevant, a black painted ball of 3 *mm* diameter is placed exactly in the laser beam. Further, the diffracted light can be attenuated in amplitude by two polarisers. The frame of reference drawn in figure 4.2 is defined from the point of view of the CCD camera. At the PC, the camera view is imaged.

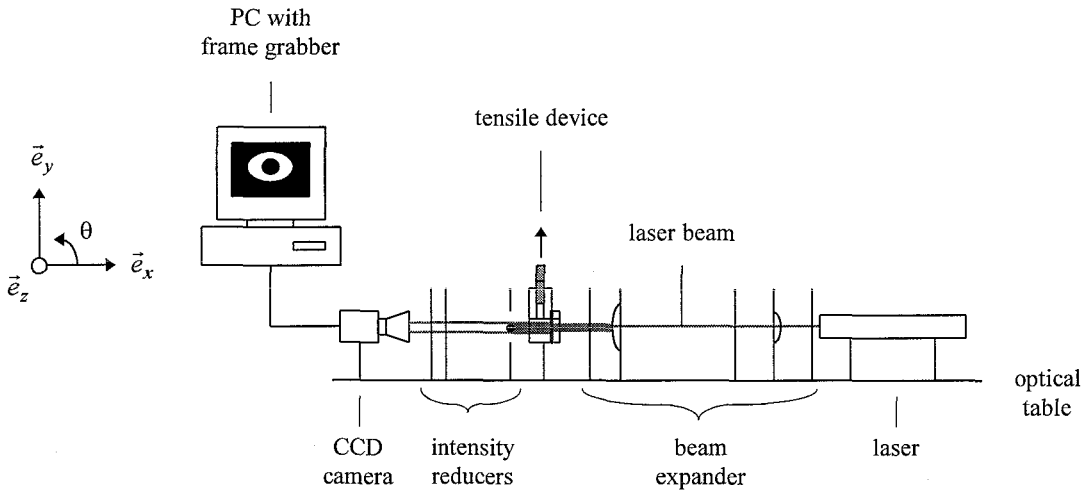

Figure 4.2: Schematic representation of the measuring system for Small Angle Light Scattering experiments. The frame of reference is defined from the point of view of the CCD camera. The arrow at the tensile device points in the direction of stretch.

4.1.2 Preparation of Skin

To obtain a bright image of the diffracted light by the collagen fibres in skin, the tissue thickness and birefringency of the collagen fibres are important.

A tissue thickness of 40 μm has been shown to yield close agreement between SALS and X-ray diffraction [Kronick & Buechler, 1986]. In human skin the collagen fibre thickness varies from 1 to 40 μm [Brown, 1972]. As tissue section thickness increases multiple scattering effects, caused by light rescattered by succeeding collagen fibre layers, become significant. An application of SALS to the mitral valve indicates that it can be used on tissues with a thickness up to 750 μm [Sacks & Chuong, 1992].

Using the strong anionic dye Sirius Red (Aldrich Chem. Co.) dissolved in aqueous Picric Acid solution (Aldrich Chem. Co.), the natural birefringency of the collagen molecules is enhanced. Besides, the tissue is preserved. Via its sulphonic acid groups, Sirius Red stains collagen by reacting with basic groups present in the collagen molecule [Junqueira et. al., 1978]. The elongated dye molecules are attached to the collagen fibre in such a way that their long axes are parallel. This relationship between dye and collagen results in an enhanced birefringency. The Sirius Red concentration is critical, values below 1 *mg/ml* (0.1%) are liable to give incomplete staining. The concentration of Picric Acid is not critical to the Sirius Red-collagen interaction, but a saturated solution avoids staining of other tissue components. The staining process is progressive with time, reaching saturation after one hour. A 0.1% solution of Sirius Red in saturated aqueous Picric Acid has a *pH* of 2 corresponding to the highest staining of collagen. However, as collagen molecules crosslink at low *pH* values, it may be better to use Sirius Red only.

4.2 Optical Characteristion of Fibre Orientation

In order to test the measuring system, verification experiments are carried out. These experiments are described in the next section. In section 4.2.2, the *in vitro* experiments for measuring collagen fibre orientation distributions in skin during deformation are described. The fibre orientation distributions are quantified in section 4.2.3, employing Lanir's fibre density function (see section 2.1.3).

4.2.1 Verification Experiments

A slice of 40 μm thick from the surface of an injection molded strip of LCP (Liquid Crystal Polymer) material is used for the verification of the SALS measurements using the measuring system as described in section 4.1.1. At the surface of the LCP strip, fibres are highly orientated in a direction parallel to the surface. In the measuring system of figure 4.2, the slice of LCP material is mounted at the position of the tensile device perpendicular to the optical axis (laser beam). It is placed with the approximate direction of its fibres at an angle, θ, of 45°, and at 135°, respectively.

The optical devices can cause errors by not standing exactly in line with the laser beam. To quantify this error the light pattern of the uninterrupted laser beam is measured as well.

4.2.2 *In Vitro* Experiments

For the aim of this research, a piece of human skin *in vitro* would be perfect. However, in this research, the SALS experiments are carried out on animal skin, because the experiments acquire expertise and the availability of human skin for these kind of experiments is not abundant.

No method is available to obtain slices of dermal tissue with a thickness smaller than 750 μm which are large enough for tensile stretch tests. For this reason, whole skin of a rat, with a thickness of 380 μm, is used. Two 16-weeks-old male Wistar rats were available after they had been subjected to an experiment to study the behaviour of muscles at the Rijksuniversteit Limburg.

At the chest of a rat, the skin and the hairs are relatively thin. As hairs diffract light, they are first removed from the skin. In order to preserve the *in vivo* configuration of a piece of skin, circular plastic frames are glued to the naked skin using cyanoacrylate resin. This is done, left and right from the chestbone of each rat. The frames have an inner diameter of 30 *mm* an outer diameter of 40 *mm* and a height of 2.5 *mm*. Figure 4.3 shows a schematic representation of the frames glued to the naked skin of a rat. The frames with the skin glued to it are removed from the rat and the subcutaneous fat is trimmed away. They are kept (and preserved) in a saturated solution of Picric Acid with 0.1% Sirius Red for more than one hour. Next, the skin is kept for one night in a 0.15 *M* NaCl solution in order to soften the epidermis which is dehydrated by the Picric Acid solution.

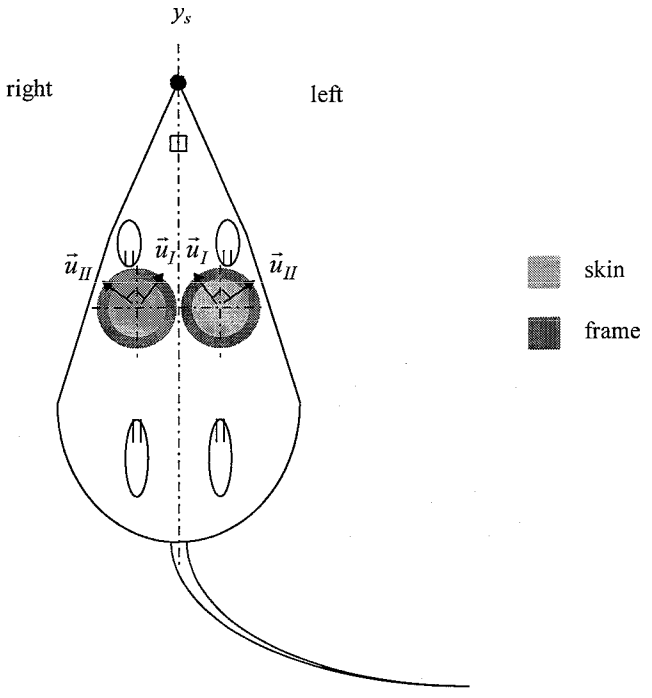

Figure 4.3: Schematic representation of a rat with plastic frames glued to the naked skin at his chest. The arrows point in the directions of stretch of Rat I and Rat II marked by $\vec{u}_I$ and $\vec{u}_{II}$, respectively. The body's axis of symmetry is marked by y_s.

Like in the *in vivo* experiments as described in section 3.2.1, the direction of stretch is applied at an angle inclined by approximately 22.5° to the preferred direction of the fibres in skin and in a direction perpendicular to this. However, no information is available about the preferred collagen fibre orientation in rat skin. To get an idea of the *in situ* collagen fibre orientation in the skin under investigation, SALS is first applied to the skin in the frame at five positions: one in the middle and at 3 *mm* above, below, right and left from the middle. The pieces of skin are positioned with the epidermis side directed to the CCD camera in a way that the Cranial direction of the skin corresponds to the y-direction of the frame of reference (see figures 4.2 and 4.3).

Now the preferred direction of the collagen fibres is known, the direction of the stretch can be applied at a certain angle to it. Each piece of skin of Rat I is stretched in a direction approximately 22.5° to the preferred orientation of the collagen fibres. Here, the right and the left side are stretched in directions approximately symmetric in regard to the body's axis of symmetry as defined in figure 4.3. The right and left pieces of skin of Rat II, are stretched in a direction approximately perpendicular to the right and left pieces of skin of Rat I. In figure 4.3, a schematic representation is given of directions of the stretch of the right and left sides of Rat I and Rat II in regard to eachother marked by $\vec{u}_I$ and $\vec{u}_{II}$, respectively. Because of the body being symmetric in regard to the breastbone, the preferred orientation angles *in situ* for the skin pieces at the right and the left side are expected to be symmetric in regard to this axis as well.

For the tensile test, the skin is cut out of the frame as shown in figure 4.4, where the solid lines are the lines of incision. The dotted lines point out the side where the skin is clenched between the serrated jaws of the tensile device. The angle between y_t and y_i depends on the measured collagen fibre orientation *in situ*, because the direction of stretch is applied in a certain direction to the preferred direction of the collagen fibres as mentioned above. In the measuring system the pieces of skin are rotated, so that the direction of stretch, marked by y_t in figure 4.4 corresponds to the direction of the y-axis as defined in figure 4.2. The broadest side is clenched in the upper serrated jaw. The width of the piece of skin is smallest in the middle (ca. 8 *mm*), in order to obtain a larger stretch at the position where the laser beam passes.

In the tensile device, the skin is stretched from 10 *mm* to 14 *mm* in 4 steps of 1 *mm* each at a speed of approximately 10^{-2} *mm/s*. The relaxation time after each state of deformation is about 60 *s*. This is significantly shorter than at the *in vivo* experiments (see section 3.2.1), but *in vitro* dermis only shows time dependent behaviour during tensile tests at strains larger than 40% [Daly, 1982].

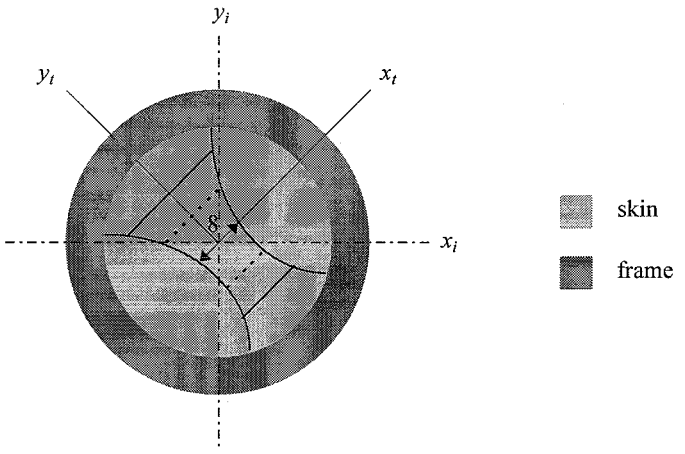

Figure 4.4: Schematic representation of *in vitro* skin of the rat isolated by a plastic frame.
The solid lines at the skin are lines of incision. The dotted lines point out the side where the skin is put between the serrated jaws of the tensile device. The dash-marked by x_i and y_i represent the x- and y-axis of the frame of reference *in situ*. The lines marked by x_t and y_t represent the frame of reference in the tensile test.

4.2.3 Quantification of Fibre Orientation Distribution

The image of the scattered light pattern recorded by the CCD camera is a map exhibiting 256 different grey levels for each pixel varying from 0 for black to 255 for white. The size of the whole image is 752×512 pixels. In order to quantify the SALS pattern, it is made binary using a threshold operation. For all the pieces of skin the same threshhold level is used. The quantification of the fibre orientation distributions from the binary images is described below.

First, the coordinates of the centre of the laser beam are determined from a measurement of the light pattern of the uninterrupted laser beam. From this point, each binary image of a SALS pattern is divided in 26 equal intervals, so $\Delta\theta = 2\pi/26$. In each interval, the pixel with the maximum radius, R_k, to the middle of the beam is selected and its polar angle, θ_k, is determined. This is schematically drawn in figure 4.5. Because of the SALS image being symmetric, the radii with an polar angle ranging from π to 2π *rad* are rotated by π *rad* and averaged with the radii with an anlge ranging from 0 to π *rad*. The averaged radii are collected in column $\underset{\sim}{R}$ and their orientation angles are collected in column $\underset{\sim}{\theta}$.

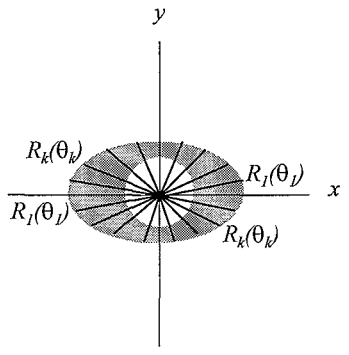

Figure 4.5: Schematic representation of a binary SALS image (grey), where the pixel with the maximum radius, R_k, to the centre of the beam (white) is selected and its angle, θ_k, is determined.

These columns of data are used for the quantification of the orientation distributions according to the density distribution function given by equation (2.6). The equation is multiplied by factor A which compensates for the size of the image. It now obtains the form:

$$R_c(\theta) = A \cdot (1/\pi + C_1(\cos^4(\theta - C_2) - 0.375)). \tag{4.1}$$

Fitting the data in equation (4.1) produces three parameters of which two are of interest, the parameters describing the orientation distribution C_1 and C_2. The calculations are performed using a Gauss-Newton iterative method (Matlab version 4.2c). The initial estimations for all measurements are set to:

$$\underset{\sim 0}{\hat{x}} = \begin{bmatrix} A_0 & C_{10} & C_{20} \end{bmatrix}^T = \begin{bmatrix} \overline{R} \cdot \pi & 0.4 & \pi/2 \end{bmatrix}^T, \tag{4.2}$$

where $\overline{R}$ is the mean of column $\underset{\sim}{R}$. The initial estimations for the parameters C_1 and C_2 are chosen rather arbitrary, but they do not influence the estimation results.

Results of Verification Experiments

The quantification of the orientation distribution of the SALS pattern obtained for the slice of LCP material with an approximate preferred fibre orientation at 135° is shown in Figure 4.6. The binary SALS image is shown in figure 4.6a. The selected pixels are shown in figure 4.6b and represented by '*'. Figure 4.6c shows the estimation results of the quantification of the orientation distribution of the SALS image. The averaged data used for the quantification of the orientation distribution are represented by '+' and the fitted function is represented by the solid line.

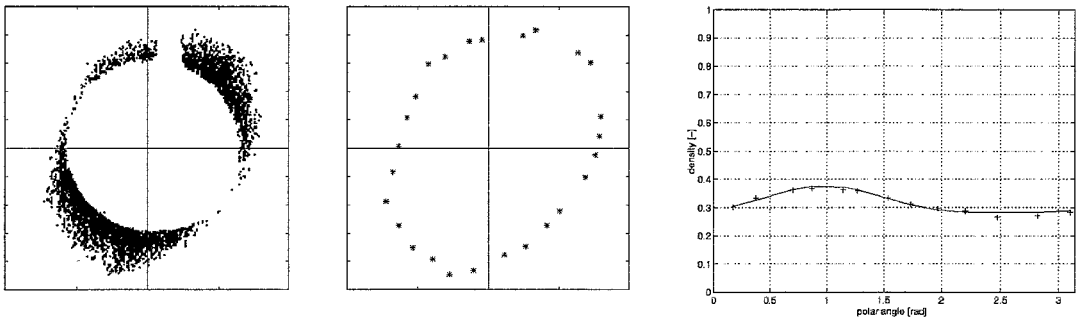

a) b) c)

Figure 4.6: Quantification of the orientation distribution of the SALS pattern of a slice of LCP material with approximate preferred fibre orientation at 135°.
a) The binary SALS image, b) selected pixels and c) measured data ('+') and fitted function (solid line).

Since light is diffracted in a direction perpendicular to the preferred orientation of the fibres, the estimated parameter C_2 from the SALS pattern is shifted by 90° (see section 2.3.1). The difference between the measured data and the calculated data, the residuals, give an indication of the reliability of the parameters. The residuals are defined by:

$$\underset{\sim}{r} = \underset{\sim}{h}(\underset{\sim}{\hat{x}}) / A - \underset{\sim}{y} / A \,, \tag{4.3}$$

where $\underset{\sim}{h}(\underset{\sim}{\hat{x}})$ represents the fit according to equation (4.1) and $\underset{\sim}{y}$ the measured data. The mean of the residuals, $\bar{r}$, and its standard deviation, s, are calculated for each measurement to give an indication of the errors. The mean of the residuals is expected to be 0 and the standard deviation is expected to be in the order of magnitude of the residual standard deviation of the data measured from the uninterrupted laser beam.

The estimation results of the verification experiments are stated in table 4.1. From this table, it can be observed that parameter C_1 and the residuals of the uninterrupted laser beam are small and thus, the laser beam radius does not show a significant deviation from a circle. The pattern of the uninterrupted laser beam is not shifted by 90°.This is an indication for the optical devices standing almost exactly in line, and thus not causing significant measuring errors. From table 4.1, it can also be observed that it is possible to estimate the preferred orientation angle, C_2, of the fibres in the LCP material by measuring SALS data using a CCD camera. However, parameter C_1, ,describing the anisotropic distribution, was expected to be higher, because the SALS patterns of the slices of LCP material seen on a piece of white paper were more orientated than was seen at the monitor.

Laser beam		LCP at 45° (0.78 *rad*)		LCP at 135° (2.35 *rad*)	
C_1 [-]	C_2 [*rad*]	C_1 [-]	C_2 [*rad*]	C_1 [-]	C_2 [*rad*]
-0.007	1.670	0.0583	0.597	0.0952	2.552
$\bar{r}$	s	$\bar{r}$	s	$\bar{r}$	s
0.0001	0.0019	0.0012	0.0068	0.0030	0.0075

Table 4.1: Estimation results of the verification experiments.
Here, C_2 is the estimated preferred orientation angle of the fibres.

Results of the *In Vitro* Experiments

Two pieces of skin failed during the experiments, therefore only the estimation results of the SALS measurements of the right side of Rat II and the left side of Rat I are presented. The estimation results of the collagen fibre orientation distribution *in situ* are stated in table 4.2. From this table, it can be observed that at most positions the measured fibre orientation distribution is not symmetrical in regard to the body's axis of symmetry, y_s, as defined in figure 4.3.

Position	Right side of Rat II		Left side of Rat I	
	C_1 [-]	C_2 [*rad*]	C_1 [-]	C_2 [*rad*]
middle	0.028	0.202	0.014	3.043
above	0.011	0.211	0.018	2.881
below	0.011	0.334	0.015	0.167
right	0.016	0.079	0.029	0.133
left	0.021	0.222	0.022	0.583

Table 4.2: Estimation results of the SALS measurements on skin of a rat *in situ*.
Here, C_2 is the estimated preferred orientation angle of the fibres.

The direction of stretch is applied at a certain angle to the preferred direction of the collagen fibres (see section 4.2.2). Here, it is based on the estimated preferred orientation angle, C_2, of the position in the middle. A piece of skin of the right side of Rat II is cut out in a way that the preferred orientation angle in the tensile device at reference state (state 0) is approximately 2.75 *rad* in regard to the frame of reference. The piece of skin of the left side of Rat I is cut out in a way that the preferred orientation angle in the tensile device at reference state is approximately 1.96 *rad*. In table 4.3, the estimation results of the pieces of skin during deformation are stated. From this table, it can be observed that the calculated values for parameter C_2 do not correspond to the expected values. Though, for all measurements the residuals are in the order of magnitude of that of the light pattern of the uninterrupted laser beam. These are indications, that the *in vitro* SALS measurements on rat skin do not contain any information about the collagen fibre orientation during deformation.

State	Right side of Rat II		Left side of Rat I	
	C_1 [-]	C_2 [*rad*]	C_1 [-]	C_2 [*rad*]
0	0.022	0.334	0.016	0.249
1	0.024	0.347	0.033	0.232
2	0.022	0.514	0.030	0.092
3	0.013	0.041	0.017	0.035
4	0.022	3.030	0.022	0.166

Table 4.3: Estimation results of the SALS measurements on skin of a rat during deformation.
Here, C_2 is the estimated preferred orientation angle of the fibres.

4.3 Discussion & Conclusions

In this chapter, it was tried to gain information about the collagen fibre orientation during deformation. For this purpose, Small Angle Light Scattering experiments were carried out on isolated pieces of rat skin *in situ* and during uniaxial deformation. Verification experiments were carried out on a slice of mainly uniaxially orientated LCP material. The SALS patterns were measured with a black & white CCD camera. These patterns were used for the quantification of the fibre orientation distributions.

Evaluation of the results of the experiments leads to the following conclusions:

- It is possible to determine the preferred fibre orientation of a slice of LCP material with a thickness of 40 μm measuring SALS data using a CCD camera.
- In case of LCP material, the calculated distribution of fibres in the preferred fibre direction is significantly smaller than expected.
- It is not possible to determine the preferred collagen fibre orientation in rat skin with a thickness of 380 μm using a CCD camera.

Summarising, it can be stated that the detection equipment used for detecting the SALS patterns is not sensitive enough. In the next chapter, recommendations are made for improved measurements of the collagen fibre orientation during deformation.

Chapter 5

Conclusions & Recommendations

In this research, the in-plane, anisotropic non-linear behaviour of human skin was characterised, employing Lanir's Skin Model.

The *in vivo* configuration and mechanical properties of collagen fibres in human skin were characterised by means of a confrontation of measured data from an experiment with calculated data from the finite element model, eventually leading to the determination of some material parameters of Lanir's Skin Model. For this purpose, two *in vivo* experiments were carried out on one isolated piece of skin at the inner side of the fore-arm at the same ambient conditions. In the first experiment, the direction of stretching was about transverse to the long axis of the fore-arm. In the second experiment, the direction of stretching was rotated by 90°. During the experiments, reaction forces of the skin and the marker positions at different states of deformation were measured. The measured reaction forces of the skin were used for the characterisation of the collagen fibre stiffness and its mean undulation. The marker positions were used for the characterisation of parameters describing the collagen fibre orientation distribution in reference state.

Evaluation of the estimation results leads to the following **conclusions**:

- From simulated 'experiments' it is concluded that the estimation process used is succesful for different initial guesses, but the speed of convergence differs. In two estimation steps for both sets of parameters, a good estimate can be obtained.
- Using the data of the Transverse experiment, the same values are found for the estimated parameters starting from different initial guesses. Therefore, the values become more reliable.
- Using the data of the Longitudinal experiment, it is only possible to determine the collagen fibre stiffness and mean undulation. Here, the estimated values for the parameters describing the collagen fibre orientation distribution of the Transverse experiment were used.
- The residuals of the reaction forces are in the expected order of magnitude. The lowest residuals are found for the longitudinal experiment. Resulting from the estimation process, the collagen fibre mean undulation, μ_c, ranges from 1.42 to 1.43 and the collagen fibre stiffness, K_c, from 50 to 90 N/mm^2. The estimated values for the collagen fibre stiffness do not differ significantly from values from literature [Savenije, 1984].
- The residuals of the marker positions are larger than expected and exhibit structure, rather than randomness. The structure for both experiments is not the same. Further, the residuals of the marker positions increase with increasing load. These are all indications that modelling errors are present.

It has to be noted that the mechanical behaviour of human skin depends on site, age, sex, and humidity. However the characterisation was restricted to one site of one test person for one ambient condition, the results obtained gain insight in the in the in-plane mechanical behaviour of human skin. The experimental set-up and the implemented skin model are useful tools to increase the knowledge on the in-plane mechanical behaviour of human skin *in vivo*. However, the skin model still exhibits some modelling errors.

Below a number of **recommendations** are stated for future research:

- Lanir's Skin Model is restricted to the characterisation of the dermis. It is questionable if the influence of the epidermis and hypodermis can be neglected. Since the hydration of the skin influences the stiffness of the epidermis significantly [Manschot, 1985], it is suggested to investigate this phenomenon. The influence of hydration of the skin is a very interesting subject in relation to all kinds of personal care products. The connection of the dermis to the hypodermis differs in different parts of the body. It is therefore suggested to incorporate the influence of the hypodermis in the constitutive model.
- The experiments performed demonstrated that the viscoelastic behaviour is of significant importance. For future research, it is recommended to incorporate viscoelastic behaviour. Since the collagen fibres demonstrate viscoelastic properties [Manschot, 1985], it is suggested to supply the collagen fibres in Lanir's Skin Model with viscoelasticity. However, this will result in an increase of computing effort. An example of a function describing viscoelastic behaviour of collagen fibres is given by Lanir [Lanir, 1983]. Some experimental data is already available, which is convenient.
- In this research, the characterisation was restricted to the mechanical behaviour of human skin in-plane. It is recommended to employ a full 3D description of skin deformation. With this the influence of the hypodermis and underlying tissues can be incorporated. It is suggested to simulate indentation tests employing Lanir' Skin Model. Experimental data of indentation tests are already available at the Personal Care Institute.
- Finally, it is recommended to carry out experiments on the face and the neck in order to obtain more consistent material parameters for the skin model for improving shaving systems. It is suggested to reconsider the anatomy of skin of the face and neck, because it is essentially different from the rest of the body, in particular musculature and the connection to the underlying tissue [Huson, 1995].

To obtain additional information about the collagen fibre orientation during deformation, Small Angle Light Scattering (SALS) was used. In SALS, laser light is passed trough a thin specimen, with a portion of incident light scattered due to the different refraction indices of the fibres and the surrounding matrix. In this research, experiments were carried out on *in vitro* isolated pieces of rat skin in the *in vivo* configuration and during deformation. Verification experiments were carried out on a slice of mainly uniaxially orientated LCP material. The SALS patterns were measured using a CCD camera. From the images obtained the fibre orientation distributions were quantified.

Evaluation of the results obtained by SALS images leads to the following **conclusions**:

- It is possible to determine the preferred fibre orientation angle of a slice of LCP material with a thickness of 40 μm by detecting SALS patterns with a CCD camera. However, the estimated parameter describing the anisotropic distribution of fibres was significantly smaller than expected.
- It is not possible to detect the portion of light scattered by stained collagen fibres in rat skin with a thickness of 380 μm using a CCD camera. According to literature, a thickness in this range would not contribute to multiple scattering effects too significantly[Sacks & Chuong, 1992].

For these reasons, it is concluded that a CCD camera is not sensitive enough for a good detection of SALS patterns. If better detection equipment is used, the SALS measuring system developed can be a useful tool for a fast characterisation of collagen fibre orientation distributions (during deformation).

Below a number of **recommendations** are stated for future research on this subject:

- For direct detection of a SALS pattern, a CCD camera is required which can measure a broader range of light intensity than the CCD camera used here. However, this option is expensive. Photographic film is a field detector as well [Yang et.al., 1987], but has the disadvantage that for quantification of the fibre orientation distribution the film-negatives have to be scanned which can only be done afterwards. Another possibility for better detection equipment is a linear array of photodiodes rotating in concentric circles around the optical axis [Sacks & Chuong, 1992].

However, the rotation of the linear array of photodiodes takes time, which is inconvenient for biological samples degenerating during the experiment.

- The collagen fibres of the rat skin were stained by a solution of 1 *mg/ml* Sirius Red in saturated aqueous Picric Acid in order to enhance their birefringency. This solution has a pH of 2. At low *pH* values it is possible that the collagen fibres crosslink changing the mechanical behaviour of the skin. However, at higher *pH* values the uptake of Sirius Red by collagen is less, and other skin components are stained too resulting in a less bright SALS pattern. Therefore, it is recommended to investigate the biochemical changes in skin caused by the staining process. An optimum between a bright SALS pattern and minimal change in mechanical behaviour is recommended. It has to be noted that Picric Acid also preserves biological tissues.
- Finally, it is recommended to carry out experiments on isolated human skin *in situ* and during deformation. To avoid significant multiple scattering effects, a thickness smaller than 750 μm is required [Sacks & Chuong, 1992]. However, human skin is thicker in most parts of the body. Besides, it is not possible to remove the epidermis from the dermis without destroying the collagen fibre structure. The epidermis will cause some extra multiple scattering effects. By means of a freezing microtome, it is possible to cut slices parallel to the skin surface, that are thin enough for SALS measurements. However, with this technique, it is hard to obtain the slices large and thick enough for a tensile test. Using a freezing microtome, it is suggested to fix pieces of skin, each stretched at a different amount, by means of chemicals [Kronick & Buechler, 1986].

References

Brown, I.A., 1971,
Structural Aspects of the Biomechanical Properties of Human Skin, Vol. I + II. Thesis, Glasgow.

Brown, I.A., 1972,
Scanning Electron Microscopy of Human Dermal Fibrous Tissue. Journal of Anatomy, Vol. 72, pp. 159-186, 1972.

Cox, H., 1941,
The Cleavage Lines of the Skin. Britisch Journal of Surgery, Vol. 29, pp. 234.

Daly, C.H., 1966,
The Biomechanical Characteristics of Human Skin. Thesis, Glasgow.

Feron, R.P.M.J., 1993,
A 3-D Structural Skin Model: Development and Implementation. Unclassified Nat.Lab. Report 024/93.

Finlay, B., 1969,
Scanning Electron Microscopy of the Human Dermis under Uniaxial Strain. Biomechanical Engineering, Vol. 4, pp. 322-327.

Hecht, E., 1987,
Optics. 2nd edition. Adelphi University, Addison-Wesley Publishing Company, New York.

Hendriks, M.A.N., 1991,
Identification of the Mechanical Behaviour of Solid Materials. Ph.D. Thesis, Eindhoven University of Technology, The Netherlands.

Huson, A., 1995,
Functionele Anatomie. Coarse 1994-1995, Eindhoven University of Technology, The Netherlands.

Junqueira, L.C.U., Bignolas G. and Bretani R.R., 1978,
Picrosirius Staining plus Polarization Microscopy, a Specific Method for Collagen Detection in Tissue Sections. Histochemical Journal, Vol. 11, pp. 447-455.

Kronick, P.L. and Buechler, P.R., 1986,
Fiber Orientation in Calfskin by Laser Light Scattering or X-Ray Diffraction and Quantitative Relation to Mechanical Properties. JALCA, Vol. 81, pp. 221-229.

Lanir, Y., 1979,
A Structural Theory for the Homogeneous Biaxial Stress-Strain Relation in Flat Collageneous Tissues. Journal of Biomechanics, Vol. 12, pp. 423-436.

Lanir, Y., 1983,
Constitutive Equations for Fibrous Connective Tissues. Journal of Biomechanics, Vol. 16, pp. 1-12.

Lanir, Y., Lichtenstein, O. and Imanuel, O., 1996,
Optimal Design of Biaxial Tests for Structural Material Characterization of Flat Tissues. Journal of Biomechanical Engineering, Vol. 118, pp. 41-47.

Langer, A.K., 1861,
Zur Anatomie und Physiology der Haut. Sitzungsbericht, Academie der Wissenschaften, Wien, 44, 19.

Manschot, J.F.M.,1985,
The Mechanical Properties of Human Skin In Vivo. Ph.D. Thesis, Nijmegen University, The Netherlands.

Montagna, W, 1965,
The Skin. Scientific American, Vol. 212 (2), pp. 56.

MARC Analysis Research Corporation, 1994,
Volumes A-E of the MARC Reference Library Manuals. reversion K.5. Palo Alto, USA.

NAG, Numerical Algorithms Group Ltd., 1993,
Version MARC 15 of the NAG Fortran Library Manual, Oxford, United Kingdom.

Oxlund, H., 1983,
Changes in Connective Tissues during Corticophin and Corticorteroid Treatment. Biomechanical Studies on Muscle Tendon, Skin and Aorta in Experimental Animals. M.D. Thesis, Anatomisk Institut, Universtiy of Aarhus, Aarhus.

Peters, G.W.M., 1987,
Tools for the Measurement of Stress and Strain Fields in Soft Tissue. Ph.D. Thesis, University of Limburg, The Netherlands.

Reihsner, R., Balog, B. and Menzel, E.J., 1995,
Two-Dimensional Elastic Properties of Human Skin in Terms of an Incremental Model at the In Vivo Configuration. Med. Eng. Phys., Vol. 17, pp.304-313.

Ridge, M.D. and Wright, V., 1966,
The Directional effect of skin - a Bio-Engineering Study of Skin with Particular Reference to Langer's Lines. Journal of Investigative Dermatology, Vol. 46, pp. 341-346.

Sacks, M.S. and Chuong, C.H., 1992,
Characterisation of Collagen Fibre Architecture in the Canine Diaphragmatic Central Tendon. Journal of Biomechanical Engineering, Vol. 114, pp. 183-190.

Savenije, E.P.W., 1982,
Structure and Mechanical Properties of Human Hair and Skin. Nat.Lab. Report No. 5806.

Smith, L., Holbrook, K., and Byers, P., 1982,
Structure of the Dermal Matrix during Development and in the Adult. Journal of Invest. Derm., Vol. 79 (suppl. 1), pp. 93s-104s.

Starmans, F.P.J., 1994,
Parfit: a Parameter Estimation Tool. Nat.Lab. Report No. 6712.

Voorden van der, W.K.L., 1996,
Characterization of the in-plane Mechanical Behaviour of Human Skin - a Mixed Numerical-Eperimental Approach Employing a Structural Skin Model. Unclassified Nat.Lab. Report 014/96.

Yang, C.F., Crosby, C.m., Eusufzai, A.R.K., and Mark, R.E., 1987,
Determination of Paper Sheet Fiber Orientation Distributions by Laser Optical Diffraction Method.
Journal of Applied Polymer Science, Vol. 34, pp. 1145-1157.

Appendix A

Parameter Estimation Algorithm

In this appendix, the algorithm used to adjust some parameters of the constitutive model employed is described.

Assume that *a priori* information on the previous (or *a priori*) estimate for the unknown parameters $\underset{\sim k}{\hat{x}}$ is available and can be modelled by:

$$\underset{\sim k}{\hat{x}} = \underset{\sim t}{x} + \underset{\sim k}{w}, \tag{A.1}$$

with $\underset{\sim t}{x}$ a column with true parameter values and $\underset{\sim k}{w}$ the column of estimation errors with zero mean and covariance matrix $\underline{P}_k$:

$$E(\underset{\sim k}{w}) = 0, \quad E(\underset{\sim k}{w}, \underset{\sim k}{w}^T) = \underline{P}_k, \tag{A.2}$$

with E the expected value operator. The non-linear model for the measured data is represented by:

$$\underset{\sim k+1}{y} = \underset{\sim k+1}{h}(\underset{\sim t}{x}) + \underset{\sim k+1}{v}. \tag{A.3}$$

The non-linear function $\underset{\sim k+1}{h}(\underset{\sim t}{x})$, symbolising the finite element calculation, describes the dependence of the $k+1^{th}$ observation on column $\underset{\sim t}{x}$. Column $\underset{\sim k+1}{y}$ contains measured data from the experiment. Column $\underset{\sim k+1}{v}$ contains measuring errors with supposed zero mean and covariance matrix $\underline{R}_{k+1}$:

$$E(\underset{\sim k+1}{v}) = 0, \quad E(\underset{\sim k+1}{v}, \underset{\sim k+1}{v}^T) = \underline{R}_{k+1}. \tag{A.4}$$

It is assumed that $\underset{\sim k}{w}$ and $\underset{\sim k+1}{v}$ are uncorrelated, thus:

$$E(\underset{\sim k}{w}\ \underset{\sim k+1}{v}^T) = 0. \tag{A.5}$$

Besides equations (A.7) and (A.8), the parameters have to obey a set of equality and inequality constraints based on physical considerations, for example:

$$b(\underset{\sim t}{x}) = 0, \quad c(\underset{\sim t}{x}) \geq 0. \tag{A.6}$$

The estimation problem is formulated as an optimisation problem and can be written as the weighted minimisation formulation:

$$\min_{\underset{\sim}{\hat{x}}_{k+1}} \left\{ (\underset{\sim}{y}_{k+1} - \underset{\sim}{h}_{k+1}(\underset{\sim}{\hat{x}}_{k+1}))^T \underline{R}_{k+1}^{-1} (\underset{\sim}{y}_{k+1} - \underset{\sim}{h}_{k+1}(\underset{\sim}{\hat{x}}_{k+1})) + (\underset{\sim}{\hat{x}}_{k} - \underset{\sim}{\hat{x}}_{k+1})^T (\underline{P}_k + \underline{Q}_k)^{-1} (\underset{\sim}{\hat{x}}_{k} - \underset{\sim}{\hat{x}}_{k+1}) \;\middle|\; b(\underset{\sim}{\hat{x}}_{k+1}) = 0 \wedge c(\underset{\sim}{\hat{x}}_{k+1}) \geq 0 \right\} . \tag{A.7}$$

It can be derived that matrix $\underline{P}_k$ is updated according to:

$$\underline{P}_{k+1} = \underline{Z}^T [\underline{Z} [\underline{H}_{k+1}^T (\underset{\sim}{\hat{x}}_{k+1}) \underline{R}_{k+1}^{-1} \underline{H}_{k+1} (\underset{\sim}{\hat{x}}_{k+1}) + (\underline{P}_k + \underline{Q}_k)^{-1}] \underline{Z}^T]^{-1} \underline{Z} . \tag{A.8}$$

The matrix $\underline{H}_{k+1}$ expresses the sensitivity of the model output for the parameter variations and is defined as:

$$\underline{H}_{k+1} = \left(\frac{\partial \underset{\sim}{h}_{k+1}(\underset{\sim}{x})}{\partial \underset{\sim}{x}} \right)_{\underset{\sim}{x} = \underset{\sim}{\hat{x}}_k} . \tag{A.9}$$

The matrix $\underline{Z}$ accounts for the active constraints. Matrix $\underline{Q}_k$ represents an artificial modelling error covariance which is added in order to assure convergence [Starmans, 1994].

The described estimator is implemented in the program PARFIT [Starmans, 1994], employing the NAG library [NAG, 1993]. The implemented algorithm is designed to minimize an arbitrary smooth function subject to constaints. Per estimation step, first the minimisation according to equation (A.7) is performed. Secondly, the estimate covariance matrix is updated according to equation (A.8). In this way a sequence of guesses for the solution (estimates) is generated, converging to the solution of the minimisation problem.

Appendix B

Numerical Parameter Analysis

In this appendix, the influence of some of the parameters of Lanir's Skin Model on the calculated reaction forces and the marker displacements in case of the skin stretch experiments are analysed. This is done by simulating the transverse as well as the longitudinal experiment for a number of different sets of parameters. The parameters describing the collagen fibre orientation distribution, C_1 and C_2, the stiffness, K_c, and the mean undulation, μ_c are varied.

B.1 Transverse Experiment Simulations

The Transverse experiment is defined as the experiment where the preferred orientation of the fibres is 22.5° (≈ 0.4 *rad*) to the x-axis (see figure 3.11). For the simulations the finite element model of the Transverse experiment, as described in section 3.2.2, is used. The parameters not varied have the same value as those used in the estimation process (see table 3.2). In table B.1, the parameter values for which the reaction forces and the marker positions are calculated are stated. The so-called true values are based on the expected values for the Transverse experiment (see section 3.2.3). The lower and higher values are based on the expected range of each parameter.

Parameter	Dim.	True value	Low value	High value
K_c	N/mm^2	100	50	150
μ_c	-	1.4	1.2	1.6
C_1	-	0.6	0.4	0.8
C_2	*rad*	0.4	0.2	0.6

Table B.1: Parameter values for which the Transverse experiment is simulated.

The influence of each parameter on the mean calculated reaction forces is shown in figure B.1.

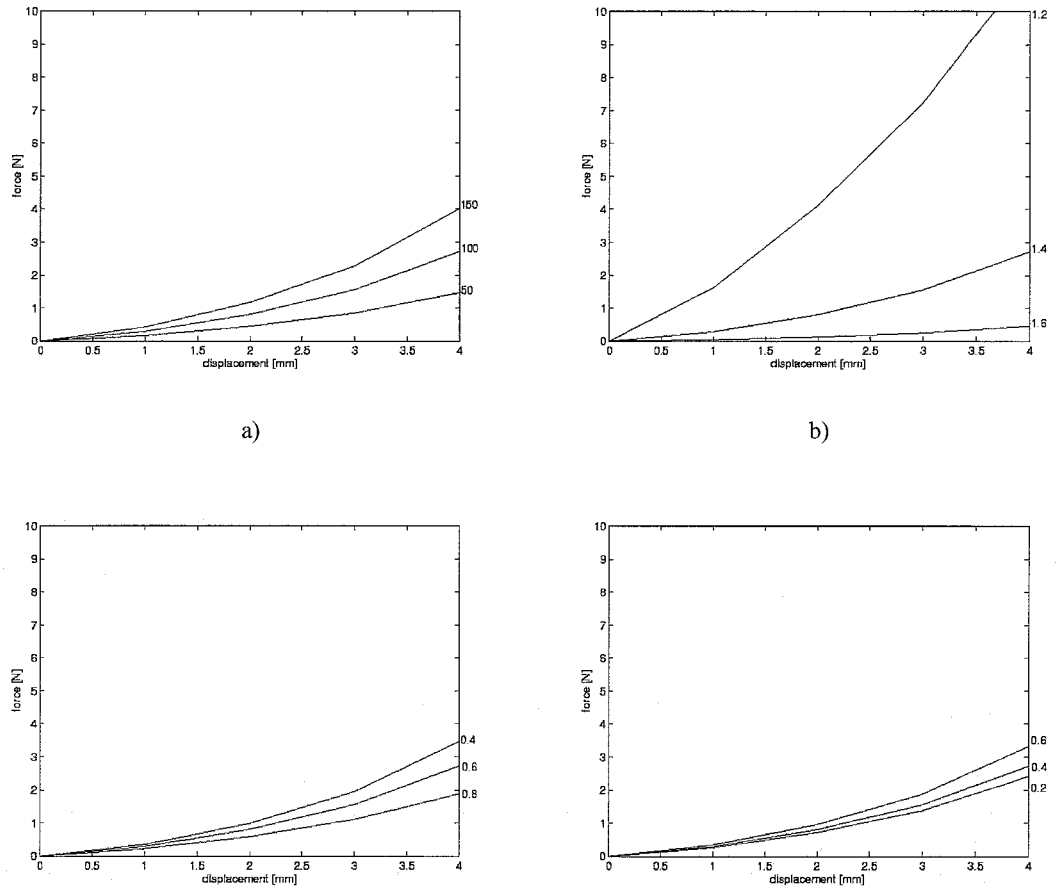

Figure B.1: Influence of parameters on the mean calculated reaction forces of the Transverse experiment. a) Parameter K_c, b) parameter μ_c, c) parameter C_1 and d) parameter C_2,.

The curve in the middle in each picture represents the mean calculated reaction forces using the true parameter values. From these pictures it appears that the reaction forces are mainly characterised by the collagen stiffness, K_c, and particularly the mean undulation, μ_c. The mean calculated reaction forces for the low and high value for μ_c differ significantly from the measured reaction forces at the end of each relaxation period (see figure 3.7a). Therefore, the range of this parameter is expected to be smaller. A better initial guess for μ_c, derived from figure B.1b, would be between 1.3 and 1.5.

The influence on the marker positions of deformation state 4 of each low parameter value is shown in figure B.2 and of each high parameter value in figure B.3. In the figures B.2 and B.3, the marker positions calculated using the true parameters are represented by 'o' and the residuals created by calculating with another value for one parameter are represented by '+'. To clarify the pictures the residuals are multiplied by a factor 10.

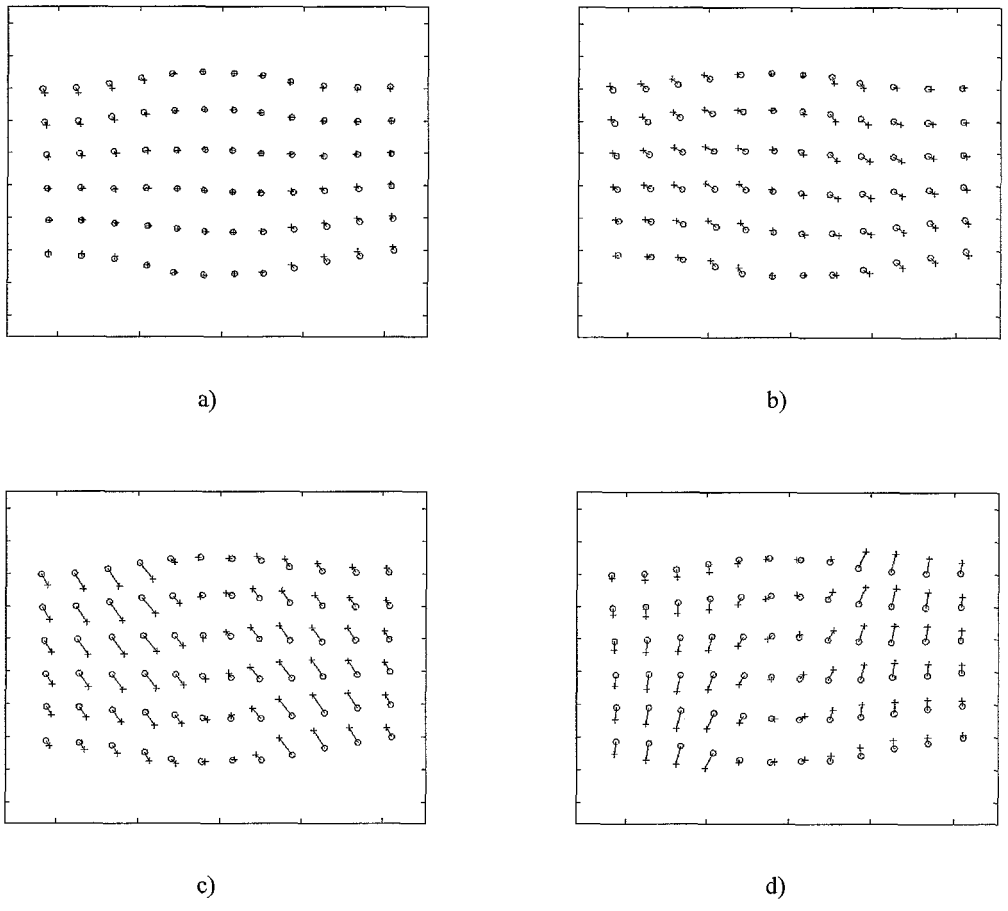

Figure B.2: Residuals of the marker positions for deformation state 4 created by a low parameter value. The marker positions calculated using the true parameters are represented by 'o'and the residual marker posisitions by '+'. The residuals are multiplied by a factor 10.
a) Parameter K_c, b) parameter μ_c, c) parameter C_1 and d) parameter C_2,.

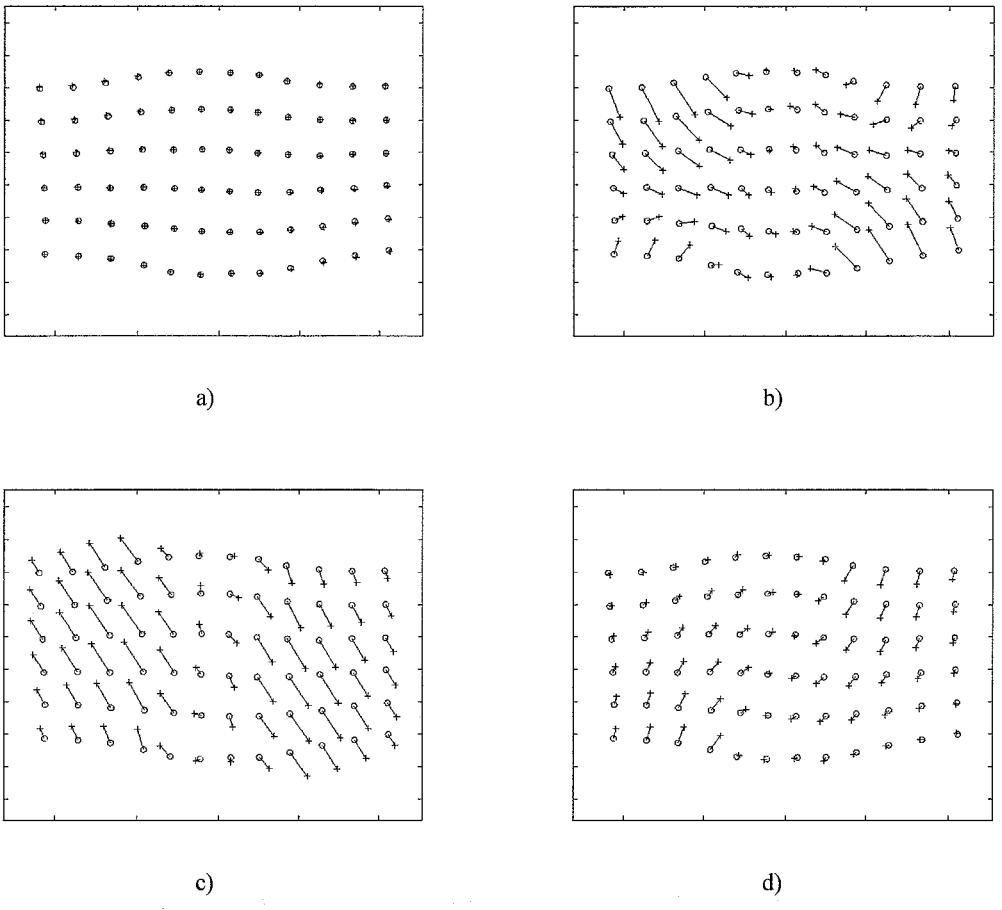

Figure B.3: Residuals of the marker positions for deformation state 4 created by a high parameter value. The marker positions calculated using the true parameters are represented by 'o'and the residual marker posisitions by '+'. The residuals are multiplied by a factor 10.
a) Parameter K_c, b) parameter μ_c, c) parameter C_1 and d) parameter C_2,.

From the figures B.2 and B.3, it can be observed that the marker displacements are mainly characterised by the collagen fibre orientation distribution parameters, C_1 and C_2, and by the mean undulation, μ_c. The marker displacements are influenced by C_1 and C_2 in approximately mutually perpendicular directions, while μ_c influences the marker displacements in almost the same direction as that of C_1. The influence of K_c on the marker displacements can be neglected.

B.2 Longitudinal Experiment Simulations

The longitudinal experiment is defined as the experiment where the preferred orientation of the fibres is 22.5° + 90° (≈ 1.95 *rad*) to the x-axis (see figure 3.11). The same calculations are done for the longitudinal experiment, except that the finite element model of the longitudinal experiment, as described in section 3.2.2, is used. In table B.2, the parameters values for which the reaction forces and the marker positions are calculated are stated. It can be observed, that only the values for C_2 differ from those in table B.1.

Parameter	Dim.	True value	Low value	High value
K_c	N/mm^2	100	50	150
μ_c	-	1.4	1.2	1.6
C_1	-	0.6	0.4	0.8
C_2	*rad*	1.95	1.75	2.15

Table B.2: Parameter values for which the longitudinal experiment is simulated.

The influence of each parameter on the mean calculated reaction forces is shown in figure B.4. Again, the curve in the middle in each picture represents the mean calculated reaction forces using the true parameter values. From these pictures it appears that, like in the Transverse experiment, the reaction forces are mainly characterised by the collagen stiffness, K_c, and particularly the mean undulation, μ_c. Here, the difference between the influences of parameters K_c and μ_c and parameters C_1 and C_2 is even larger than in the simulations of the Transverse experiment (see figure B.1). The mean calculated reaction forces for the low and high value for μ_c differ significantly from the measured reaction forces at the end of each relaxation period.

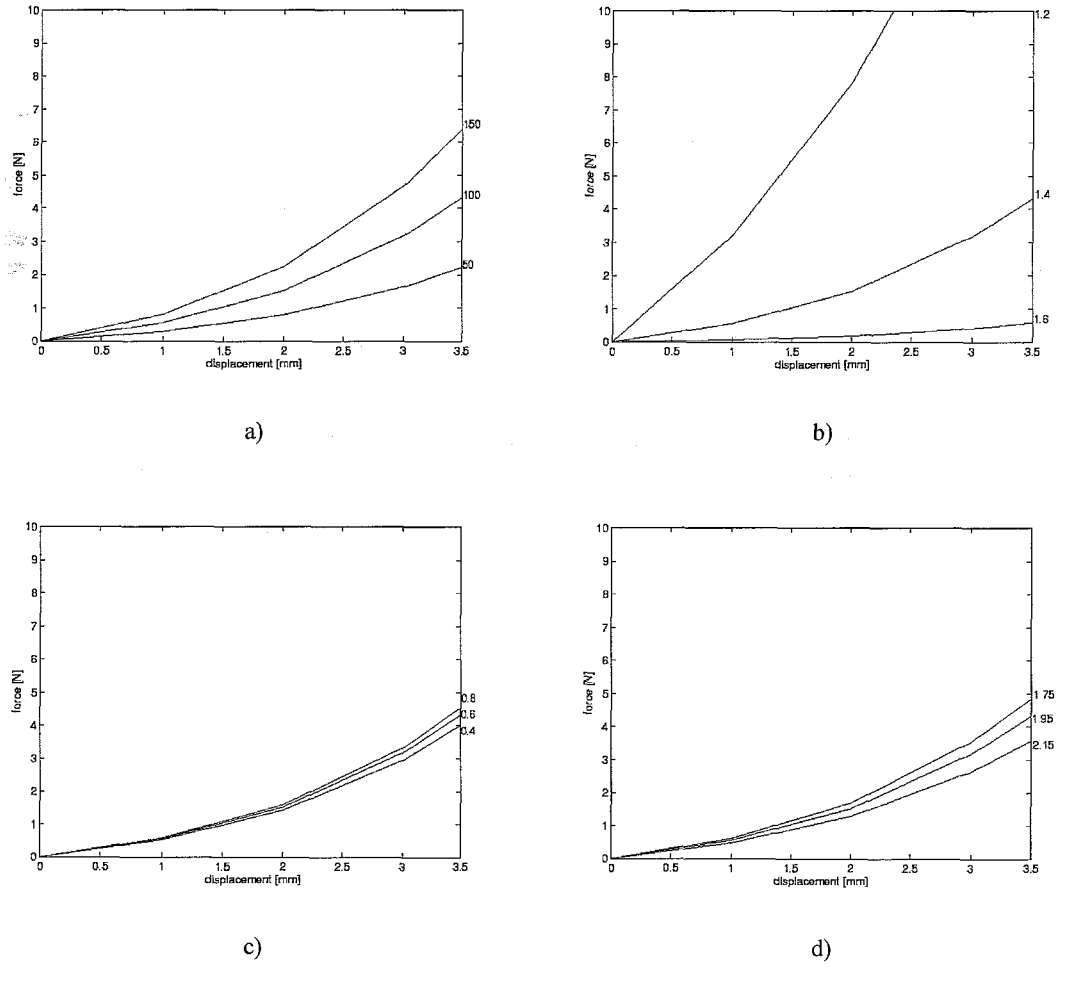

Figure B.4: Influence of parameters on the mean calculated reaction forces of the longitudinal experiment. a) Parameter K_c, b) parameter μ_c, c) parameter C_1 and d) parameter C_2,.

The influence on the marker positions of deformation state 4 of each low parameter value is shown in figure B.5 and of each high parameter value in figure B.6. In the figures B.5 and B.6, the marker positions calculated using the true parameters are again represented by 'o' and the residuals created by calculating with another value for one parameter are represented by '+'. To clarify the pictures the residuals are again multiplied by a factor 10.

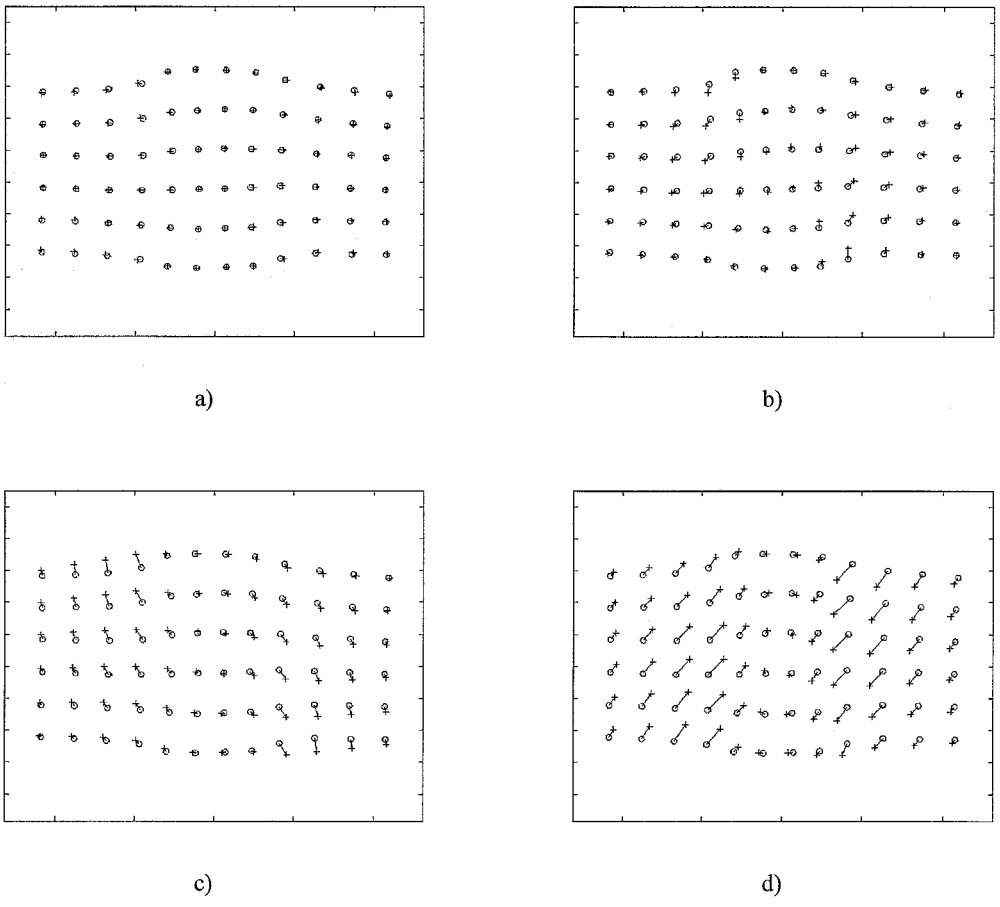

Figure B.5: Residuals of the marker positions for deformation state 4 created by a low parameter value. The marker positions calculated using the true parameters are represented by 'o'and the residual marker posisitions by '+'. The residuals are multiplied by a factor 10.
a) Parameter K_c, b) parameter μ_c, c) parameter C_1 and d) parameter C_2,.

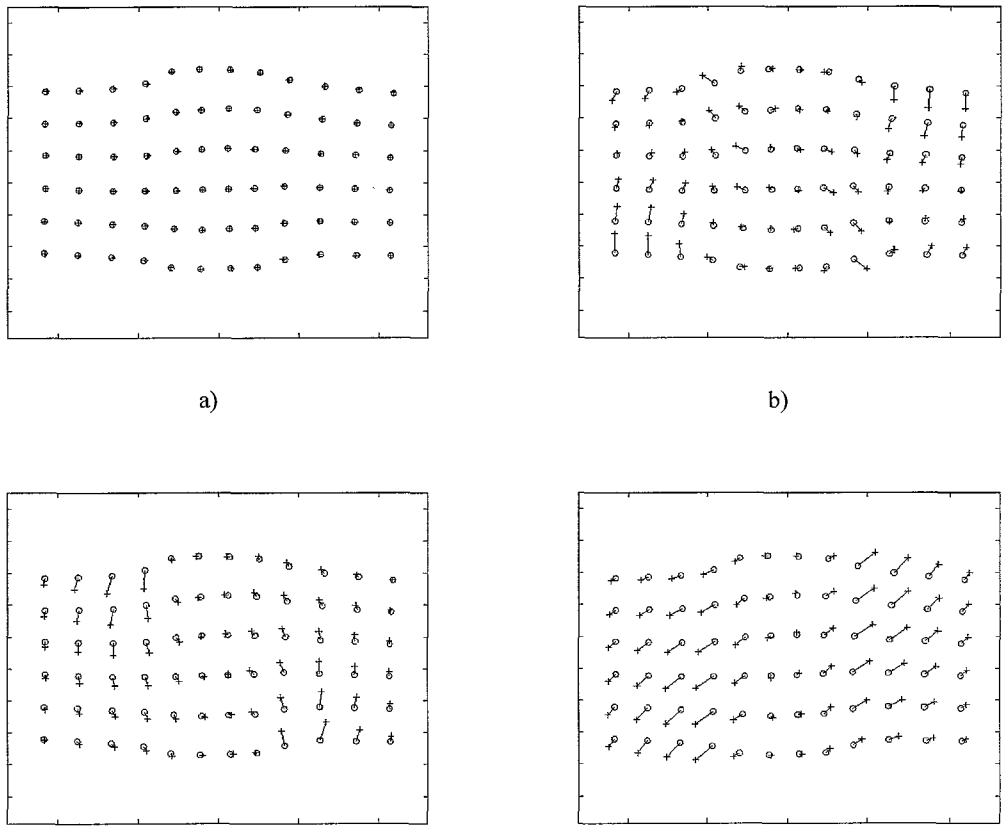

Figure B.6: Residuals of the marker positions for deformation state 4 created by a high parameter value. The marker positions calculated using the true parameters are represented by 'o'and the residual marker posisitions by '+'. The residuals are multiplied by a factor 10.
a) Parameter K_c, b) parameter μ_c, c) parameter C_1 and d) parameter C_2,.

From the figures B.5 and B.6, it can be observed that again the marker displacements are mainly characterised by the collagen fibre orientation distribution parameters, C_1 and C_2, and by the mean undulation, μ_c. And again the marker displacements are influenced by C_1 and C_2 in approximately mutually perpendicular directions and the influence of K_c on the marker displacements can be neglected. From figure B.5, it can be observed that μ_c influences the marker displacements in approximately the same direction as that of C_2 for low parameter values. From figure B.6, it can be observed that μ_c influences the marker displacements in approximately the same direction as that of C_1 for high parameter values. The influence on the marker displacements of a low and high value for μ_c differs in direction, unlike in the simulations of the Transverse experiment.